
Manifold Denoising by Nonlinear Robust Principal Component Analysis

He Lyu, Ningyu Sha, Shuyang Qin, Ming Yan, Yuying Xie, Rongrong Wang
 Department of Computational Mathematics, Science and Engineering
 Michigan State University
 {lyuhe, shaninyu, qinshuya, myan, xyy, wangron6}@msu.edu

Abstract

This paper extends robust principal component analysis (RPCA) to nonlinear manifolds. Suppose that the observed data matrix is the sum of a sparse component and a component drawn from some low dimensional manifold. Is it possible to separate them by using similar ideas as RPCA? Is there any benefit in treating the manifold as a whole as opposed to treating each local region independently? We answer these two questions affirmatively by proposing and analyzing an optimization framework that separates the sparse component from the manifold under noisy data. Theoretical error bounds are provided when the tangent spaces of the manifold satisfy certain incoherence conditions. We also provide a near optimal choice of the tuning parameters for the proposed optimization formulation with the help of a new curvature estimation method. The efficacy of our method is demonstrated on both synthetic and real datasets.

1 Introduction

Manifold learning and graph learning are nowadays widely used in computer vision, image processing, and biological data analysis on tasks such as classification, anomaly detection, data interpolation, and denoising. In most applications, graphs are learned from the high dimensional data and used to facilitate traditional data analysis methods such as PCA, Fourier analysis, and data clustering [7, 9, 10, 16, 13]. However, the quality of the learned graph may be greatly jeopardized by outliers which cause instabilities in all the aforementioned graph assisted applications.

In recent years, several methods have been proposed to handle outliers in nonlinear data [12, 23, 3]. Despite the success of those methods, they only aim at detecting the outliers instead of correcting them. In addition, very few of them are equipped with theoretical analysis of the statistical performances. In this paper, we propose a novel non-task-driven algorithm for the mixed noise model in (1) and provide theoretical guarantees to control its estimation error. Specifically, we consider the mixed noise model as

$$\tilde{X}_i = X_i + S_i + E_i, \quad i = 1, \dots, n, \quad (1)$$

where $X_i \in \mathbb{R}^p$ is the noiseless data independently drawn from some manifold \mathcal{M} with an intrinsic dimension $d \ll p$, E_i is the i.i.d. Gaussian noise with small magnitudes, and S_i is the sparse noise with possibly large magnitudes. If S_i has a large entry, then the corresponding \tilde{X}_i is usually considered as an outlier. The goal of this paper is to simultaneously recover X_i and S_i from \tilde{X}_i , $i = 1, \dots, n$.

There are several benefits in recovering the noise term S_i along with the signal X_i . First, the support of S_i indicates the locations of the anomaly, which is informative in many applications. For example, if X_i is the gene expression data from the i th patient, the nonzero elements in S_i indicate the differentially expressed genes that are the candidates for personalized medicine. Similarly, if S_i is a

result of malfunctioned hardware, its nonzero elements indicate the locations of the malfunctioned parts. Secondly, the recovery of S_i allows the “outliers” to be pulled back to the data manifold instead of simply being discarded. This prevents a waste of information and is especially beneficial in cases where data is insufficient. Thirdly, in some applications, the sparse S_i is a part of the clean data rather than a noise term, then the algorithm provides a natural decomposition of the data into a sparse and a non-sparse component that may carry different pieces of information.

Along a similar line of research, Robust Principle Component Analysis (RPCA) [2] has received considerable attention and has demonstrated its success in separating data from sparse noise in many applications. However, its assumption that the data lies in a low dimensional subspace is somewhat strict. In this paper, we generalize the Robust PCA idea to the non-linear manifold setting. The major new components in our algorithm are: 1) an incorporation of the manifold curvature information into the optimization framework, and 2) a unified way to apply RPCA to a collection of tangent spaces of the manifold.

2 Methodology

Let $\tilde{X} = [\tilde{X}_1, \dots, \tilde{X}_n] \in \mathbb{R}^{p \times n}$ be the noisy data matrix containing n samples. Each sample is a vector in \mathbb{R}^p independently drawn from (1). The overall data matrix \tilde{X} has the representation

$$\tilde{X} = X + S + E$$

where X is the clean data matrix, S is the matrix of the sparse noise, and E is the matrix of the Gaussian noise. We further assume that the clean data X lies on some manifold \mathcal{M} embedded in \mathbb{R}^p with a small intrinsic dimension $d \ll p$ and the samples are sufficient ($n \geq p$). The small intrinsic dimension assumption ensures that data is locally low dimensional so that the corresponding local data matrix is of low rank. This property allows the data to be separated from the sparse noise.

The key idea behind our method is to handle the data locally. We use the k Nearest Neighbors (k NN) to construct local data matrices, where k is larger than the intrinsic dimension d . For a data point $X_i \in \mathbb{R}^p$, we define the local patch centered at it to be the set consisted of its k NN and itself, and a local data matrix $X^{(i)}$ associated with this patch is $X^{(i)} = [X_{i_1}, X_{i_2}, \dots, X_{i_k}, X_i]$, where X_{i_j} is the j th-nearest neighbor of X_i . Let \mathcal{P}_i be the restriction operator to the i th patch, i.e., $\mathcal{P}_i(X) = \tilde{X}P_i$ where P_i is the $n \times (k+1)$ matrix that selects the columns of X in the i th patch. Then $X^{(i)} = \mathcal{P}_i(X)$. Similarly, we define $S^{(i)} = \mathcal{P}_i(S)$, $E^{(i)} = \mathcal{P}_i(E)$ and $\tilde{X}^{(i)} = \mathcal{P}_i(\tilde{X})$.

Since each local data matrix $X^{(i)}$ is nearly of low rank and S is sparse, we can decompose the noisy data matrix into low-rank parts and sparse parts through solving the following optimization problem

$$\begin{aligned} \{\hat{S}, \{\hat{S}^{(i)}\}_{i=1}^n, \{\hat{L}^{(i)}\}_{i=1}^n\} &= \arg \min_{S, S^{(i)}, L^{(i)}} F(S, \{S^{(i)}\}_{i=1}^n, \{L^{(i)}\}_{i=1}^n) \\ &\equiv \arg \min_{S, S^{(i)}, L^{(i)}} \sum_{i=1}^n (\lambda_i \|\tilde{X}^{(i)} - L^{(i)} - S^{(i)}\|_F^2 + \|\mathcal{C}(L^{(i)})\|_* + \beta \|S^{(i)}\|_1) \\ &\text{subject to } S^{(i)} = \mathcal{P}_i(S), \end{aligned} \quad (2)$$

here we take $\beta = \max\{k+1, p\}^{-1/2}$ as in RPCA, $\tilde{X}^{(i)} = \mathcal{P}_i(\tilde{X})$ is the local data matrix on the i th patch and \mathcal{C} is the centering operator that subtracts the column mean: $\mathcal{C}(Z) = Z(I - \frac{1}{k+1}\mathbf{1}\mathbf{1}^T)$, where $\mathbf{1}$ is the $(k+1)$ -dimensional column vector of all ones. Here we are decomposing the data on each patch into a low-rank part $L^{(i)}$ and a sparse part $S^{(i)}$ by imposing the nuclear norm and entry-wise ℓ_1 norm on $L^{(i)}$ and $S^{(i)}$, respectively. There are two key components in this formulation: 1). the local patches are overlapping (for example, the first data point X_1 may belong to several patches). Thus, the constraint $S^{(i)} = \mathcal{P}_i(S)$ is particularly important because it ensures copies of the same point on different patches (and those of the sparse noise on different patches) remain the same. 2). we do not require $L^{(i)}$ to be restrictions of a universal L to the i th patch, because the $L^{(i)}$ s correspond to the local affine tangent spaces, and there is no reason for a point on the manifold to have the same projection on different tangent spaces. This seemingly subtle difference has a large impact on the final result.

If the data only contains sparse noise, i.e., $E = 0$, then $\hat{X} \equiv \tilde{X} - \hat{S}$ is the final estimation for X . If $E \neq 0$, we apply Singular Value Hard Thresholding [6] to truncate $\mathcal{C}(\tilde{X}^{(i)} - \mathcal{P}_i(S))$ and remove

the Gaussian noise (See §6), and use the resulting $\hat{L}_{\tau^*}^{(i)}$ to construct a final estimate \hat{X} of X via least squares fitting

$$\hat{X} = \arg \min_{Z \in \mathbb{R}^{p \times n}} \sum_{i=1}^n \lambda_i \| \mathcal{P}_i(Z) - \hat{L}_{\tau^*}^{(i)} \|_F^2. \quad (3)$$

The following discussion revolves around (2) and (3), and the structure of the paper is as follows. In §3, we explain the geometric meaning of each term in (2). In §4, we establish theoretical recovery guarantees for (2) which justifies our choice of β and allows us to theoretically choose λ . The calculation of λ uses the curvature of the manifold, so in §5, we provide a simple method to estimate the average manifold curvature and the method is robust to sparse noise. The optimization algorithms that solve (2) and (3) are presented in §6 and the numerical experiments are in §7.

3 Geometric explanation

We provide a geometric intuition for the formulation (2). Let us write the clean data matrix $X^{(i)}$ on the i th patch in its Taylor expansion along the manifold,

$$X^{(i)} = X_i 1^T + T^{(i)} + R^{(i)}, \quad (4)$$

where the Taylor series is expanded at X_i (the center point of the i th patch), $T^{(i)}$ stores the first order term and its columns lie in the tangent space of the manifold at X_i , and $R^{(i)}$ contains all the higher order terms. The sum of the first two terms $X_i 1^T + T^{(i)}$ is the linear approximation to $X^{(i)}$ that is unknown if the tangent space is not given. This linear approximation precisely corresponds to the $L^{(i)}$ s in (2), i.e., $L^{(i)} = X_i 1^T + T^{(i)}$. Since the tangent space has the same dimensionality d as the manifold, with randomly chosen points, we have with probability one, that $\text{rank}(T^{(i)}) = d$. As a result, $\text{rank}(L^{(i)}) = \text{rank}(X_i 1^T + T^{(i)}) \leq d + 1$. By the assumption that $d < \min\{p, k\}$, we know that $L^{(i)}$ is indeed low rank.

Combing (4) with $\tilde{X}^{(i)} = X^{(i)} + S^{(i)} + E^{(i)}$, we find the misfit term $\tilde{X}^{(i)} - L^{(i)} - S^{(i)}$ in (2) equals $E^{(i)} + R^{(i)}$. This implies that the misfit contains the high order residues (i.e., the linear approximation error) and the Gaussian noise.

4 Theoretical choice of tuning parameters

To establish the error bound, we need a coherence condition on the tangent spaces of the manifold.

Definition 4.1 Let $U \in \mathbb{R}^{m \times r}$ ($m \geq r$) be a matrix with $U^*U = I$, the coherence of U is defined as

$$\mu(U) = \frac{m}{r} \max_{k \in \{1, \dots, m\}} \|U^* \mathbf{e}_k\|_2^2,$$

where \mathbf{e}_k is the k th element of the canonical basis. For a subspace T , its coherence is defined as

$$\mu(V) = \frac{m}{r} \max_{k \in \{1, \dots, m\}} \|V^* \mathbf{e}_k\|_2^2,$$

where V is an orthonormal basis of T . The coherence is independent of the choice of basis.

The following theorem is proved for local patches constructed using the ϵ -neighborhoods. We use k NN in the experiments because k NN is more robust to insufficient samples. The full version of Theorem 4.2 can be found in the appendix.

Theorem 4.2 [succinct version] Let each $X_i \in \mathbb{R}^p$, $i = 1, \dots, n$, be independently drawn from a compact manifold $\mathcal{M} \subseteq \mathbb{R}^p$ with an intrinsic dimension d and endowed with the uniform distribution. Let X_{i_j} , $j = 1, \dots, k_i$ be the k_i points falling in an η -neighborhood of X_i with radius η , where $\eta > 0$ is some fixed small constant. These points form the matrix $X^{(i)} = [X_{i_1}, \dots, X_{i_{k_i}}, X_i]$. For any $q \in \mathcal{M}$, let T_q be the tangent space of \mathcal{M} at q and define $\bar{\mu} = \sup_{q \in \mathcal{M}} \mu(T_q)$. Suppose the support of the noise matrix $S^{(i)}$ is uniformly distributed among all sets of cardinality m_i . Then as long as $d < \rho_r \min\{\underline{k}, p\} \bar{\mu}^{-1} \log^{-2} \max\{\bar{k}, p\}$, and $m_i \leq 0.4 \rho_s p \underline{k}$ (here ρ_r and ρ_s are positive constants,

$\bar{k} = \max_i k_i$, and $\underline{k} = \min_i k_i$, then with probability over $1 - c_1 n \max\{\underline{k}, p\}^{-10} - e^{-c_2 \underline{k}}$ for some constants c_1 and c_2 , the minimizer \hat{S} to (2) with weights

$$\lambda_i = \frac{\min\{k_i + 1, p\}^{1/2}}{\epsilon_i}, \quad \beta_i = \max\{k_i + 1, p\}^{-1/2} \quad (5)$$

has the error bound

$$\sum_i \|\mathcal{P}_i(\hat{S}) - S^{(i)}\|_{2,1} \leq C\sqrt{pn\bar{k}}\|\epsilon\|_2.$$

Here $\epsilon_i = \|\tilde{X}^{(i)} - X_i 1^T - T^{(i)} - S^{(i)}\|_F$ will be estimated in the next section, $\epsilon = [\epsilon_1, \dots, \epsilon_n]$, $\|\cdot\|_{2,1}$ stands for taking ℓ_2 norm along columns and ℓ_1 norm along rows, and $T^{(i)}$ is the projection of $X^{(i)} - X_i 1^T$ to the tangent space T_{X_i} .

Remark. We can interpret ϵ as the total noise in the data. As explained in §3, $\|\tilde{X}^{(i)} - X_i 1^T - T^{(i)} - S^{(i)}\|_F = \|R^{(i)} + E^{(i)}\|_F$, thus $\epsilon = 0$ if the manifold is linear and the Gaussian noise is absent. The factor \sqrt{n} in front of $\|\epsilon\|_2$ takes into account the use of different norms on the two hand sides (the right hand side is the Frobenius norm of the noise matrix $\{R^{(i)} + E^{(i)}\}_{i=1}^n$ obtained by stacking the $R^{(i)} + E^{(i)}$ associated with each patch into one big matrix). The factor \sqrt{p} is due to the small weight β_i of $\|S^{(i)}\|_1$ compared to the weight 1 on $\|\tilde{X}^{(i)} - L^{(i)} - S^{(i)}\|_F^2$. The factor \bar{k} appears because on average, each column of $\hat{S} - S$ is added about $k := \frac{1}{n} \sum_i k_i$ times on the left hand side.

5 Estimating the curvature

The definition λ_i in (5) involves an unknown quantity $\epsilon_i^2 = \|\tilde{X}^{(i)} - X_i 1^T - T^{(i)} - S^{(i)}\|_F^2 \equiv \|R^{(i)} + E^{(i)}\|_F^2$. We assume the standard deviation σ of the i.i.d. Gaussian entries of $E^{(i)}$ is known, so $\|E^{(i)}\|_F^2$ can be approximated. Since $R^{(i)}$ is independent of $E^{(i)}$, the cross term $\langle R^{(i)}, E^{(i)} \rangle$ is small. Our main task is estimating $\|R^{(i)}\|_F^2$, the linear approximation error defined in §3. At local regions, second order terms dominates the linear approximation residue, hence estimating $\|R^{(i)}\|_F^2$ requires the curvature information.

5.1 A short review of related concepts in Riemannian geometry

The principal curvatures at a point on a high dimensional manifold are defined as the singular values of the second fundamental forms [11]. As estimating all the singular values from the noisy data may not be stable, we are only interested in estimating the mean curvature, that is the root mean squares of the principal curvatures.

For the simplicity of illustration, we review the related concepts using the 2D surface \mathcal{M} embedded in \mathbb{R}^3 (Figure 1). For any curve $\gamma(s)$ in \mathcal{M} parametrized by arclength with unit tangent vector $t_\gamma(s)$, its curvature is the norm of the covariant derivative of t_γ : $\|dt_\gamma(s)/ds\| = \|\gamma''(s)\|$. In particular, we have the following decomposition

$$\gamma''(s) = k_g(s)\hat{v}(s) + k_n(s)\hat{n}(s),$$

where $\hat{n}(s)$ is the unit normal direction of the manifold at $\gamma(s)$ and \hat{v} is the direction perpendicular to $\hat{n}(s)$ and $t_\gamma(s)$, i.e., $\hat{v} = \hat{n} \times t_\gamma(s)$. The coefficient $k_n(s)$ along the normal direction is called the normal curvature, and the coefficient $k_g(s)$ along the perpendicular direction \hat{v} is called the geodesic curvature. The principal curvatures purely depend on k_n . In particular, in 2D, the principal curvatures are precisely the maximum and minimum of k_n among all possible directions.

A natural way to compute the normal curvature is through geodesic curves. The geodesic curve between two points is the shortest curve connecting them. Therefore geodesic curves are usually viewed as “straight lines” on the manifold. The geodesic curves have the favorable property that their curvatures have 0 contribution from k_g . That is to say, the second order derivative of the geodesic curve parameterized by the arclength is exactly k_n .

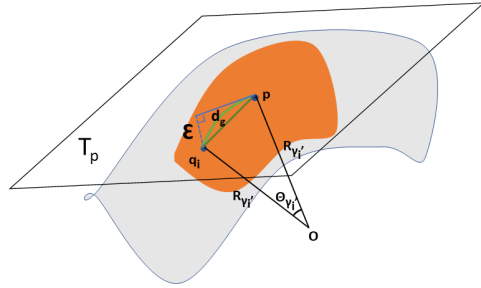


Figure 1: Local manifold geometry

Figure 1: Local manifold geometry. In particular, in 2D, the principal curvatures are precisely the maximum and minimum of k_n among all possible directions.

Algorithm 1: Estimate the mean curvature $\bar{\Gamma}(p)$ at some point p

Input: Distance matrix D , adjacency matrix A , some proper constants $r_1 < r_2$, number of pairs m

Output: the estimated mean curvature $\bar{\Gamma}(p)$

- 1 **for** $i = 1: m$ **do**
 - 2 Randomly pick some point $q_i \in B(p, r_2) \setminus B(p, r_1)$;
 - 3 Calculate the geodesic distance $d_g(p, q_i)$ using A ;
 - 4 Solve for the radius R_i based on (7);
 - 5 **end**
 - 6 Compute estimated curvature $\bar{\Gamma}(p) = (\frac{1}{m} \sum_{i=1}^m R_i^{-2})^{1/2}$.
-

Algorithm 2: Estimate the overall curvature $\bar{\Gamma}(\Omega)$ for some region Ω

Input: Distance matrix D , adjacency matrix A , some proper constants $r_1 < r_2$, number of pairs m

Output: the estimated overall curvature $\bar{\Gamma}(\Omega)$

- 1 **for** $i = 1: m$ **do**
 - 2 Randomly pick a pair of points $p_i, q_i \in \Omega$ such that $r_1 \leq d(p_i, q_i) \leq r_2$;
 - 3 Calculate the geodesic distance $d_g(p_i, q_i)$ using A ;
 - 4 Solve for the radius R_i based on (7);
 - 5 **end**
 - 6 Compute estimated curvature $\bar{\Gamma}(\Omega) = (\frac{1}{m} \sum_{i=1}^m R_i^{-2})^{1/2}$.
-

5.2 The proposed method

All existing curvature estimation methods we are aware of are in the field of computer vision where the objects are 2D surfaces in 3D [5, 4, 20, 15]. Most of these methods are difficult to generalize to high (> 3) dimensions with the exception of the integral invariant based approaches [18]. However, the integral invariant based approaches is not robust to sparse noise and is unsuited to our problem.

We propose a new method to estimate the mean curvature from the noisy data. Although the graphic illustration is made in 3D, the method is dimension independent. To compute the average normal curvature at a point $p \in \mathcal{M}$, we randomly pick m points $q_i \in \mathcal{M}$ on the manifold lying within a proper distance to p as specified in Algorithm 1. Let γ_i be the geodesic curve between p and q_i . For each i , we compute the pairwise Euclidean distance $\|p - q_i\|_2$ and the pairwise geodesic distance $d_g(p, q_i)$ using the Dijkstra's algorithm. Through a circular approximation of the geodesic curve as drawn in Figure 1, we can compute the curvature of the geodesic curve as the inverse of the radius

$$\|\gamma_i'(p)\| = 1/R_{\gamma_i'}, \quad (6)$$

where γ_i' is the tangent direction along which the curvature is calculated and $R_{\gamma_i'}$ is the radius of the circular approximation to the curve γ at p , which can be solved along with the angle $\theta_{\gamma_i'}$ through the geometric relations

$$2R_{\gamma_i'} \sin(\theta_{\gamma_i'}/2) = \|p - q_i\|_2, \quad R_{\gamma_i'} \theta_{\gamma_i'} = d_g(p, q_i), \quad (7)$$

as indicated in Figure 1. Finally, we define the average curvature $\bar{\Gamma}(p)$ at p to be

$$\bar{\Gamma}(p) := (\mathbb{E}_{q_i} \|\gamma_i'(p)\|^2)^{1/2} \equiv (\mathbb{E}_{q_i} R_{\gamma_i'}^{-2})^{1/2}. \quad (8)$$

To estimate the mean curvature from the data, we construct two matrices D and A . $D \in \mathbb{R}^{n \times n}$ is the pairwise distance matrix, where D_{ij} denotes the Euclidean distance between two points X_i and X_j . A is a type of adjacency matrix defined as follows and is to be used to compute the pairwise geodesic distances from the data,

$$A_{ij} = \begin{cases} D_{ij} & \text{if } X_j \text{ is in the } k \text{ nearest neighbors of } X_i \\ 0 & \text{elsewhere.} \end{cases} \quad (9)$$

Algorithm 1 estimates the mean curvature at some point p and Algorithm 2 estimates the overall curvature within some region Ω on the manifold.

The geodesic distance is computed using the Dijkstra's algorithm, which is not accurate when p and q are too close to each other. The constant r_1 in Algorithm 1 and 2 is thus used to make sure that p and q are sufficiently apart. The constant r_2 is to make sure that q is not too far away from p , as after all we are computing the mean curvature around p .

5.3 Estimating λ_i from the mean curvature

We provide a way to approximate λ_i when the number of points n is finite. In the asymptotic limit ($k \rightarrow \infty, k/n \rightarrow 0$), all the approximate sign “ \approx ” below become “ $=$ ”.

Fix a point $p \in \mathcal{M}$ and another point q_i in the η -neighborhood of p . Let γ_i be the geodesic curve between them. With the computed curvature $\bar{\Gamma}(p)$, we can estimate the linear approximation error of expanding q_i at p : $q_i \approx p + P_{T_p}(q_i - p)$, where P_{T_p} is the projection onto the tangent space at p . Let \mathcal{E} be the error of this linear approximation $\mathcal{E}(q_i, p) = q_i - p - P_{T_p}(q_i - p) = P_{T_p^\perp}(q_i - p)$ where T_p^\perp is the orthogonal complement of the tangent space. From Figure 1, the relation between $\|\mathcal{E}(p, q_i)\|_2$, $\|p - q_i\|_2$, and $\theta_{\gamma'_i}$ is

$$\|\mathcal{E}(p, q_i)\|_2 \approx \|p - q_i\|_2 \sin \frac{\theta_{\gamma'_i}}{2} = \frac{\|p - q_i\|_2^2}{2R_{\gamma'_i}}. \quad (10)$$

To obtain a closed-form formula for \mathcal{E} , we assume that for the fixed p and a randomly chosen q_i in an ξ neighborhood of p , the projection $P_{T_p}(q_i - p)$ follows a uniform distribution in a ball with radius η' (in fact $\eta' \approx \eta$ since when η is small, the projection of $q - p$ is almost $q - p$ itself, therefore the radius of the projected ball almost equal to the radius of the original neighborhood). Under this assumption, let $r_i = \|P_{T_p}(q_i - p)\|_2$ be the magnitude of the projection and $\phi_i = P_{T_p}(q_i - p) / \|P_{T_p}(q_i - p)\|_2$ be the direction, by [21], r_i and ϕ_i are independent of each other. As the curvature $R_{\gamma'_i}$ only depends on the direction, the numerator and the denominator of the right hand side of (10) are independent of each other. Therefore,

$$\mathbb{E}\|\mathcal{E}(p, q_i)\|_2^2 \approx \mathbb{E} \frac{\|p - q_i\|_2^4}{4R_{\gamma'_i}^2} = \frac{\mathbb{E}\|p - q_i\|_2^4}{4} \mathbb{E}R_{\gamma'_i}^{-2} = \frac{\mathbb{E}\|p - q_i\|_2^4}{4} \cdot \bar{\Gamma}^2(p), \quad (11)$$

where the first equality used the independence and the last equality used the definition of the mean curvature in the previous subsection.

Now we apply this estimation to the neighborhood of X_i . Let $p = X_i$, and $q_j = X_{i_j}$ be the neighbors of X_i . Using (11), the average linear approximation error on this patch is

$$\frac{1}{k} \|R^{(i)}\|_F^2 := \frac{1}{k} \sum_{j=1}^k \|\mathcal{E}(X_{i_j}, X_i)\|_2^2 \xrightarrow{k \rightarrow \infty} \frac{\mathbb{E}\|X_i - X_{i_j}\|_2^4}{4} \bar{\Gamma}^2(X_i), \quad (12)$$

where the right hand side can also be estimated with

$$\frac{1}{k} \sum_{j=1}^k \frac{\|X_i - X_{i_j}\|_2^4}{4} \bar{\Gamma}^2(X_i) \xrightarrow{k \rightarrow \infty} \frac{\mathbb{E}\|X_i - X_{i_j}\|_2^4}{4} \bar{\Gamma}^2(X_i) \quad (13)$$

so when k is sufficient large, $\frac{1}{k} \|R^{(i)}\|_F^2$ is also close to $\frac{1}{k} \sum_{j=1}^k \frac{\|X_i - X_{i_j}\|_2^4}{4} \bar{\Gamma}^2(X_i)$, which can be completely computed from the data. Combining this with the argument at the beginning of §5 we get,

$$\epsilon_i = \|R^{(i)} + E^{(i)}\|_F \approx \sqrt{\|R^{(i)}\|_F^2 + \|E^{(i)}\|_F^2} \approx \left((k+1)p\sigma^2 + \sum_{j=1}^k \frac{\|X_i - X_{i_j}\|_2^4}{4} \bar{\Gamma}^2(X_i) \right)^{1/2} =: \hat{\epsilon}.$$

Thus we can set $\hat{\lambda}_i = \frac{\min\{k+1, p\}^{1/2}}{\hat{\epsilon}_i}$ due to (5). We show in the appendix that $\left| \frac{\hat{\lambda}_i - \lambda_i^*}{\lambda_i^*} \right| \xrightarrow{k \rightarrow \infty} 0$, where $\lambda_i^* = \frac{\min\{k+1, p\}^{1/2}}{\epsilon_i}$ as in (5).

6 Optimization algorithm

To solve the convex optimization problem (2) in a memory-economic way, we first write $L^{(i)}$ as a function of S and eliminate them from the problem. We can do so by fixing S and minimizing the objective function with respect to $L^{(i)}$

$$\begin{aligned} \hat{L}^{(i)} &= \arg \min_{L^{(i)}} \lambda_i \|\tilde{X}^{(i)} - L^{(i)} - S^{(i)}\|_F^2 + \|\mathcal{C}(L^{(i)})\|_* \\ &= \arg \min_{L^{(i)}} \lambda_i \|\mathcal{C}(L^{(i)}) - \mathcal{C}(\tilde{X}^{(i)} - S^{(i)})\|_F^2 + \|\mathcal{C}(L^{(i)})\|_* + \lambda_i \|(I - \mathcal{C})(L^{(i)} - (\tilde{X}^{(i)} - S^{(i)}))\|_F^2. \end{aligned} \quad (14)$$

Notice that $L^{(i)}$ can be decomposed as $L^{(i)} = \mathcal{C}(L^{(i)}) + (I - \mathcal{C})(L^{(i)})$, set $A = \mathcal{C}(L^{(i)})$, $B = (I - \mathcal{C})(L^{(i)})$, then (14) is equivalent to

$$(\hat{A}, \hat{B}) = \arg \min_{A, B} \lambda_i \|A - \mathcal{C}(\tilde{X}^{(i)} - S^{(i)})\|_F^2 + \|A\|_* + \lambda_i \|B - (I - \mathcal{C})(\tilde{X}^{*(i)} - S^{(i)})\|_F^2,$$

which decouples into

$$\hat{A} = \arg \min_A \lambda_i \|A - \mathcal{C}(\tilde{X}^{(i)} - S^{(i)})\|_F^2 + \|A\|_*, \quad \hat{B} = \arg \min_B \lambda_i \|B - (I - \mathcal{C})(\tilde{X}^{(i)} - S^{(i)})\|_F^2.$$

The problems above have closed form solutions

$$\hat{A} = \mathcal{T}_{1/2\lambda_i}(\mathcal{C}(\tilde{X}^{(i)} - \mathcal{P}_i(S))), \quad \hat{B} = (I - \mathcal{C})(\tilde{X}^{(i)} - \mathcal{P}_i(S)) \quad (15)$$

where \mathcal{T}_μ is the soft-thresholding operator on the singular values

$$\mathcal{T}_\mu(Z) = U \max\{\Sigma - \mu I, 0\} V^*, \quad \text{where } U\Sigma V^* \text{ is the SVD of } Z.$$

Combing \hat{A} and \hat{B} , we have derived the closed form solution for $\hat{L}^{(i)}$

$$\hat{L}^{(i)}(S) = \mathcal{T}_{1/2\lambda_i}(\mathcal{C}(\tilde{X}^{(i)} - \mathcal{P}_i(S))) + (I - \mathcal{C})(\tilde{X}^{(i)} - \mathcal{P}_i(S)). \quad (16)$$

Plugging (16) into F in (2), the resulting optimization problem solely depends on S . Then we apply FISTA [1, 19] to find the optimal solution \hat{S} with

$$\hat{S} = \arg \min_S F(\hat{L}^{(i)}(S), S). \quad (17)$$

Once \hat{S} is found, if the data has no Gaussian noise, then the final estimation for X is $\hat{X} \equiv \tilde{X} - \hat{S}$; if there is Gaussian noise, we use the following denoised local patches $\hat{L}_{\tau^*}^{(i)}$

$$\hat{L}_{\tau^*}^{(i)} = H_{\tau^*}(\mathcal{C}(\tilde{X}^{(i)} - \mathcal{P}_i(\hat{S}))) + (I - \mathcal{C})(\tilde{X}^{(i)} - \mathcal{P}_i(\hat{S})), \quad (18)$$

where H_{τ^*} is the Singular Value Hard Thresholding Operator with the optimal threshold as defined in [6]. This optimal thresholding removes the Gaussian noise from $\hat{L}_{\tau^*}^{(i)}$. With the denoised $\hat{L}_{\tau^*}^{(i)}$, we solve (3) to obtain the denoised data

$$\hat{X} = \left(\sum_{i=1}^n \lambda_i \hat{L}_{\tau^*}^{(i)} P_i^T \right) \left(\sum_{i=1}^n \lambda_i P_i P_i^T \right)^{-1}. \quad (19)$$

The proposed Nonlinear Robust Principle Component Analysis (NRPCA) algorithm is summarized in Algorithm 3. There is one caveat in solving (2): the strong sparse noise may result in a wrong

Algorithm 3: Nonlinear Robust PCA

Input: Noisy data matrix \tilde{X} , k (number of neighbors in each local patch), T (number of neighborhood updates iterations)

Output: the denoised data \hat{X} , the estimated sparse noise \hat{S}

- 1 Estimate the curvature using (8);
 - 2 Estimate λ_i , $i = 1, \dots, n$ as in §5, set β as in (2);
 - 3 $\hat{S} \leftarrow 0$;
 - 4 **for** $iter = 1: T$ **do**
 - 5 Find the k NN for each point using $\tilde{X} - \hat{S}$ and construct the restriction operators $\{\mathcal{P}_i\}_{i=1}^n$;
 - 6 Construct the local data matrices $\tilde{X}^{(i)} = \mathcal{P}_i(\tilde{X})$ using \mathcal{P}_i and the noisy data \tilde{X} ;
 - 7 $\hat{S} \leftarrow$ minimizer of (17) iteratively using FISTA;
 - 8 **end**
 - 9 Compute each $\hat{L}_{\tau^*}^{(i)}$ from (18) and assign \hat{X} from (19).
-

neighborhood assignment when constructing the local patches. Therefore, once \hat{S} is obtained and removed from the data, we update the neighborhood assignment and re-compute \hat{S} . This procedure is repeated T times.

7 Numerical experiment

Simulated Swiss roll: We demonstrate the superior performance of NRPCA on a synthetic dataset following the mixed noise model (1). We sampled 2000 noiseless data X_i uniformly from a 3D Swiss roll and generated the Gaussian noise matrix with i.i.d. entries obeying $\mathcal{N}(0, 0.25)$. The sparse noise matrix S is generated by randomly replacing 100 entries of a zero $p \times n$ matrix with i.i.d. samples generated from $(-1)^y \cdot z$ where $y \sim \text{Bernoulli}(0.5)$ and $z \sim \mathcal{N}(5, 0.09)$. We applied NRPCA to the simulated data with patch size $k = 15$. Figure 2 reports the denoising results in the original space (3D) looking down from above. We compare two ways of using the outputs of NRPCA: 1). only remove the sparse noise from the data $\tilde{X} - \hat{S}$; 2). remove both the sparse and Gaussian noise from the data: \hat{X} . In addition, we plotted $\tilde{X} - \hat{S}$ with and without the neighbourhood update. These results are all superior to an ad-hoc application of the Robust PCA on the individual local patches.

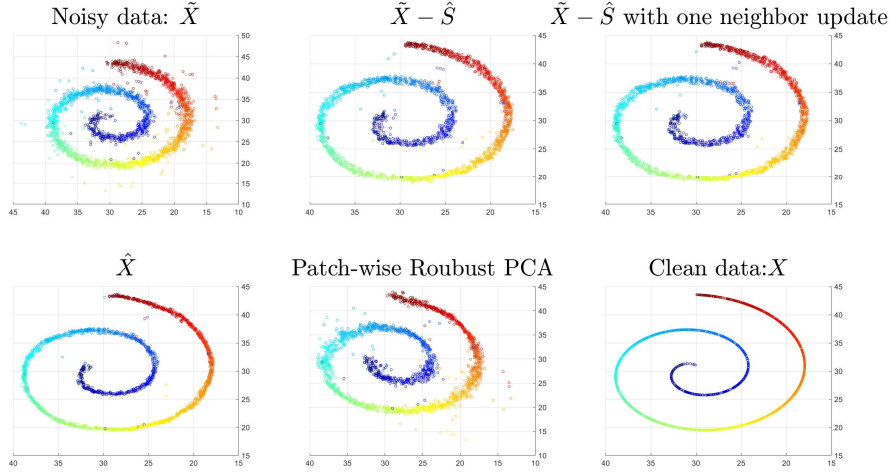


Figure 2: NRPCA applied to the noisy 3D Swiss roll dataset. $\tilde{X} - \hat{S}$ is the result after subtracting the sparse noise estimated by setting $T = 1$ in NRPCA, i.e., no neighbour update; “ $\tilde{X} - \hat{S}$ with one neighbor update” used the \hat{S} obtained by setting $T = 2$ in NRPCA; clearly, the neighbour update helped to remove more sparse noise; \hat{X} is the data obtained via fitting the denoised tangent spaces as in (3). Compared to “ $\tilde{X} - \hat{S}$ with one neighbor update”, it further removed the Gaussian noise from the data; “Patch-wise Robust PCA” refers to the ad-hoc application of the vanilla Robust PCA to each local patch independently, whose performance is worse than the proposed joint-recovery formulation.

High dimensional Swiss roll: We carried out the same simulation on a high dimension Swiss roll, and obtained better distinguishability among 1)-3). We also observed an overall improvement of the performance of NRPCA, which matches our intuition that the assumptions of Theorem 4.2 are more likely to be satisfied in high dimensions. The denoised results are displayed in Figure 3, where we clearly see that the use of \hat{X} instead of $\tilde{X} - \hat{S}$ allows a significant amount of Gaussian noise to be removed from the data.

In the high dimensional simulation, we generated a Swiss roll in \mathbb{R}^{20} as following:

1. Choose the number of samples $n = 2000$;
2. let t be the vector of length n containing the n uniform grid points in the interval $[0, 4\pi]$ with grid space $4\pi/(n - 1)$;
3. Set the first three dimensions of the data the same way as the 3D Swiss roll, for $i = 1, \dots, n$,

$$\begin{aligned} X_i(1) &= (t(i) + 1) \cos(t(i)); \\ X_i(2) &= (t(i) + 1) \sin(t(i)); \\ X_i(3) &\sim \text{unif}([0, 8\pi]), \end{aligned}$$

where $\text{unif}([0, 8\pi])$ means the uniform distribution on the interval $[0, 8\pi]$.

4. Set the 4-20 dimensions of the data to contain pure sinusoids with various frequencies

$$X_i(k) = t(i) \sin(f_k t(i)), \quad k = 4, \dots, 20, .$$

where $f_k = k/21$ is the frequency for the k th dimension. The noisy data is obtained by adding i.i.d. Gaussian noise $\mathcal{N}(0, 0.25)$ to each entry of X and adding sparse noise to 600 randomly chosen entries where the noise added to each chosen entry obeys $\mathcal{N}(5, 0.09)$.

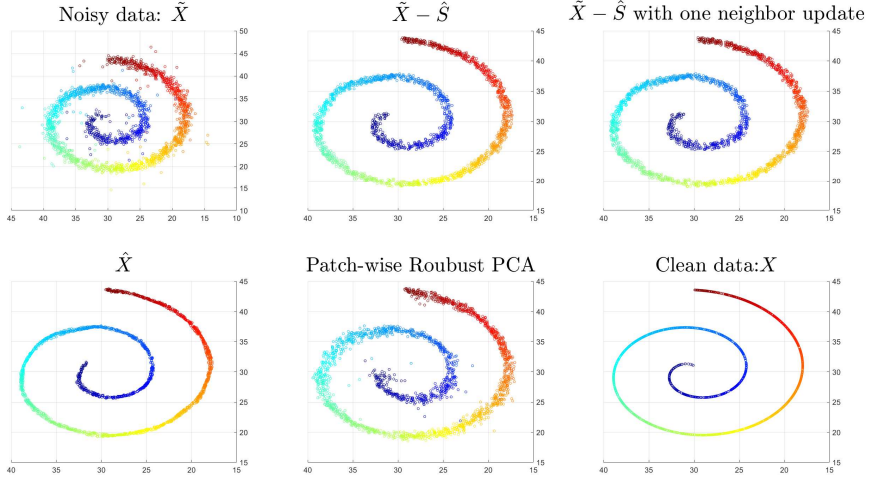


Figure 3: NRPCA applied to the noisy 20D Swiss roll data set. $\tilde{X} - \hat{S}$ is the result after subtracting the estimated sparse noise via NRPCA with $T = 1$; “ $\tilde{X} - \hat{S}$ with one neighbor update” is that with $T = 2$, i.e., patches are reassigned once; \hat{X} is the denoised data obtained via fitting the tangent spaces in NRPCA with $T = 2$; “Patch-wise Robust PCA” refers to the ad-hoc application of the vanilla RPCA to each local patch independently, whose performance is clearly worse than the proposed joint-recovery formulation.

MNIST: We observe some interesting dimension reduction results of the MNIST dataset with the help of NRPCA. It is well-known that the handwritten digits 4 and 9 have so high a similarity that some popular dimension reduction methods, such as Isomap and Laplacian Eigenmaps (LE) are not able to separate them into two clusters (first column of Figure 4). Despite the similarity, a few other methods (such as t-SNE) are able to distinguish them to a much higher degree, which suggests the possibility of improving the results of Isomap and LE with proper data pre-processing. We conjecture that the overlapping parts in Figure 4 (the left column) are caused by personalized writing styles with different beginning or finishing strokes. This type of differences can be better modelled by sparse noise than Gaussian or Poisson noises. The right columns of Figure 4 confirm this conjecture: after the NRPCA denoising (with $k = 10$), we see a much better separability of the two digits using the first two coordinates of Isomap and Laplacian Eigenmaps. Here we used 2000 randomly drawn images of 4 and 9 from the MNIST training dataset. Figure 5 used another random set of the same cardinality and $k = 5$, but they both demonstrated that the denoising step greatly facilitates the dimensionality reduction.

In addition, we observe some emerging trajectory (or skeleton) patterns in the plot of the denoised embedding (right column of Figure 4 and Figure 5). Mathematically speaking, this is due to the nuclear norm penalty on the tangent spaces in the optimization formulation that forces the denoised data to have a small intrinsic dimension. However, since the small intrinsic dimensionality is not manually inputted but implicitly imposed via an automatic calculation of the data curvature and the weight parameter λ_i , we do not think the trajectory pattern is a human artifact. To further examine the meaning the trajectories, we replaced the dots in the bottom two scattered plots in Figure 5 by their original images of the digits, and obtained Figure 6 and Figure 7. We can see that 1). the digits are better grouped in the denoised embedding than the original one and 2). the trajectories in the denoised

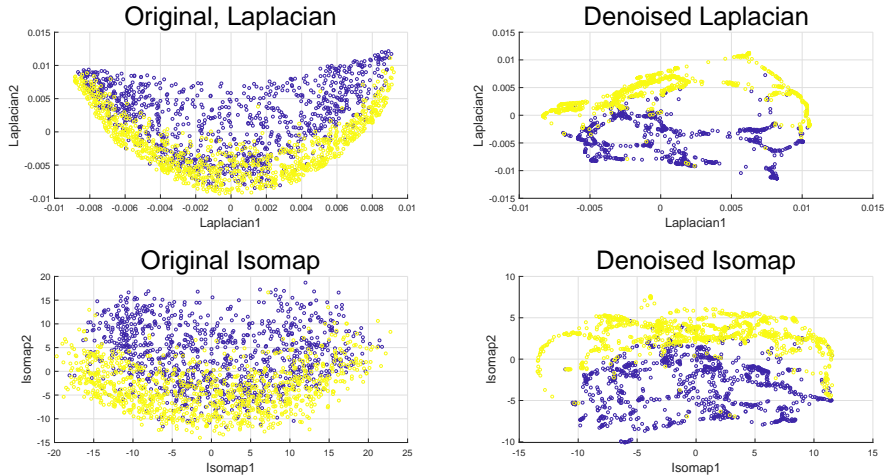


Figure 4: Laplacian eigenmaps and Isomap results for the original and the NRPCA denoised digits 4 and 9 from the MNIST dataset.

embedding correspond to gradual transitions between the two images on the two ends. If two images are connected by two trajectories, then it indicates two ways for one image to gradually deform into the other. Furthermore, Figure 8 listed a few images of 4 and 9 before and after denoising, which shows which part of the image is detected as sparse noise and changed by NRPCA.

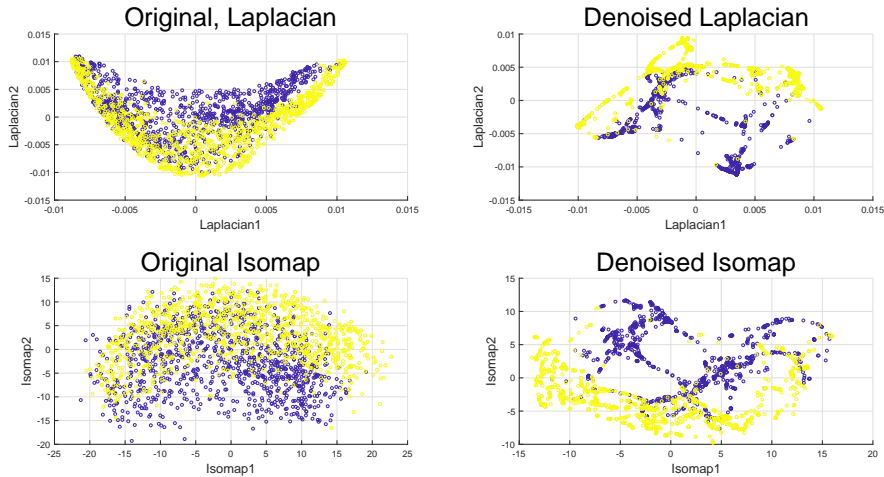


Figure 5: Laplacian eigenmaps and Isomap results for the original and the NRPCA denoised digits 4 and 9 from the MNIST dataset.

Figure 9 shows the results for NRPCA denoising with more iterations of patch-reassignment, we can see that the results almost have no visible difference after $T > 2$. Since the patch-reassignment is in the outer iteration, increasing its frequency greatly increases the computation time. Fortunately, we find that often times two iterations are enough to deliver a good denoising result.

Biological data: We illustrate the potential usefulness of NRPCA algorithm on an embryoid body (EB) differentiation dataset over a 27-day time course, which consists of gene expressions for 31,000 cells measured with single-cell RNA-sequencing technology (scRNAseq) [14, 17]. This EB data comprising expression measurement for cells originated from embryoid at different stages is hence developmental in nature, which should exhibit a progressive type of characters such as tree structure because all cells arise from a single oocyte and then develop into different highly-differentiated

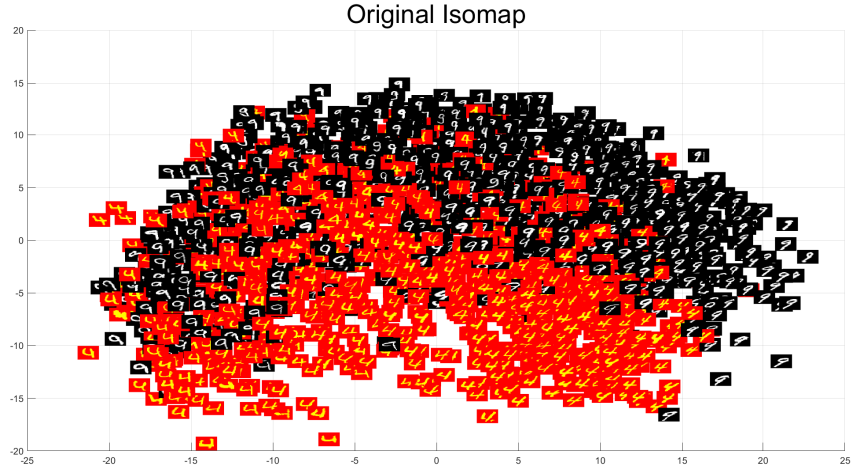


Figure 6: Isomap embedding using the original data from the MNIST dataset.

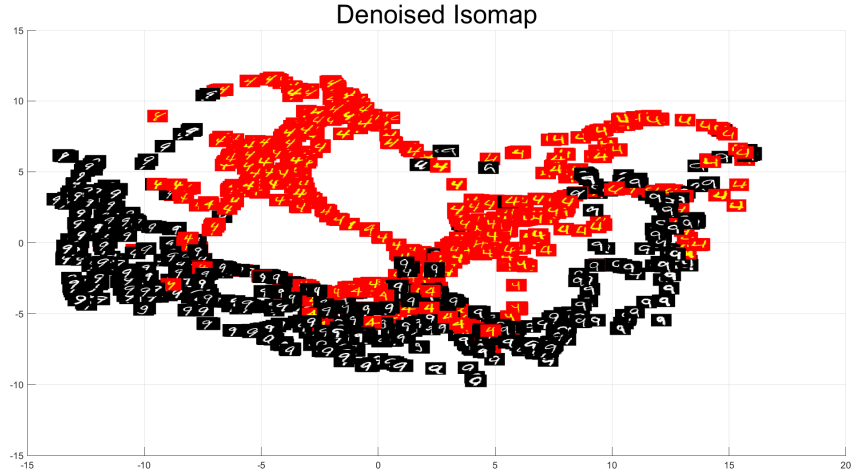


Figure 7: Isomap embedding using the Denoised data via NRPCA.

tissues. This progression character is often missing when we directly apply dimension reduction methods to the data as shown in Figure 10 because biological data including scRNAseq is highly noisy and often is contaminated with outliers from different sources including environmental effects and measurement error. In this case, we aim to reveal the progressive nature of the single-cell data from transcript abundance as measured by scRNAseq.

We first normalized the scRNAseq data following the procedure described in [17] and randomly selected 1000 cells using the stratified sampling framework to maintain the ratios among different developmental stages. We applied our NRPCA method to the normalized subset of EB data and then applied Locally Linear Embeddin (LLE) to the denoised results. The two-dimensional LLE results are shown in Figure 10. Our analysis demonstrated that although LLE is unable to show the progression structure using noisy data, after the NRPCA denoising, LLE successfully extracted the trajectory structure in the data, which reflects the underlying smooth differentiating processes of embryonic cells. Interestingly, using the denoised data from $\bar{X} - \hat{S}$ with neighbor update, the LLE embedding showed a branching at around day 9 and increased variance in later time points, which was confirmed by manual analysis using 80 biomarkers in [17].

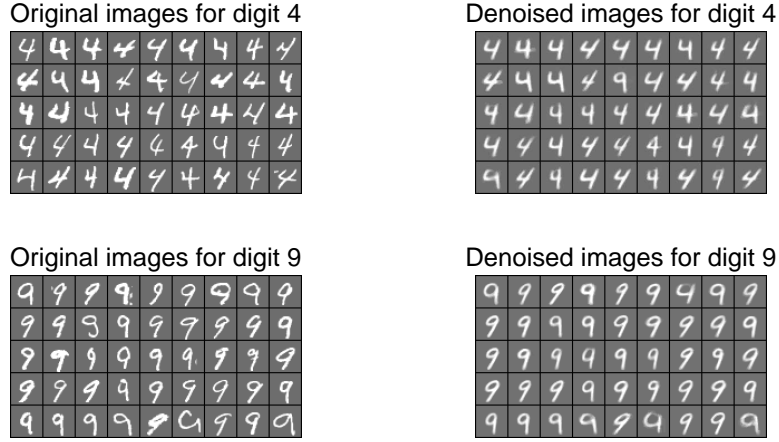


Figure 8: A comparison of the original and the NRPCA denoised images of digit 4 and 9.

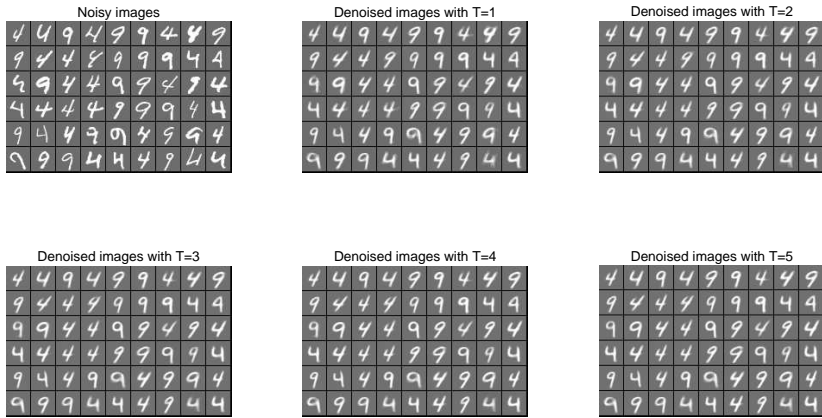


Figure 9: NRPCA Denoising results with more iterations of patch-reassignment.

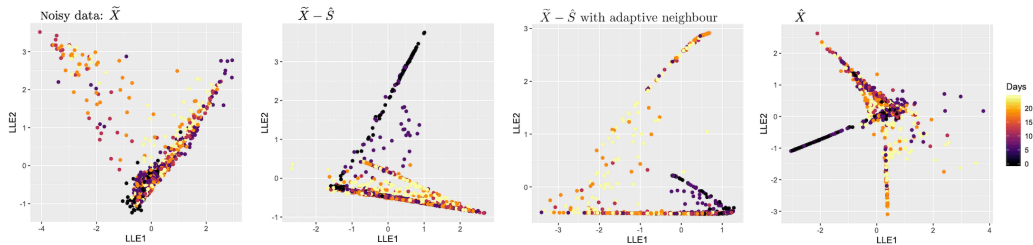


Figure 10: LLE results for denoised scRNAseq data set.

8 Conclusion

In this paper, we proposed the first outlier correction method for nonlinear data analysis that can correct outliers caused by the addition of large sparse noise. The method is a generalization of the Robust PCA method to the nonlinear setting. We provided procedures to treat the non-linearity by working with overlapping local patches of the data manifold and incorporating the curvature

information into the denoising algorithm. We established a theoretical error bound on the denoised data that holds under conditions only depending on the intrinsic properties of the manifold. We tested our method on both synthetic and real dataset that were known to have nonlinear structures and reported promising results.

Acknowledgements The authors would like to thank Shuai Yuan, Hongbo Lu, Changxiong Liu, Jonathan Fleck, Yichen Lou, and Lijun Cheng for useful discussions. This work was supported in part by the NIH grants U01DE029255, 5RO3DE027399 and the NSF grants DMS-1902906, DMS-1621798, DMS-1715178, CCF-1909523 and NCS-1630982.

References

- [1] Amir Beck and Marc Teboulle. A fast iterative shrinkage-thresholding algorithm for linear inverse problems. *SIAM journal on imaging sciences*, 2(1):183–202, 2009.
- [2] Emmanuel J. Candes, Xiaodong Li, Yi Ma, and John Wright. Robust Principal Component Analysis? *J. ACM*, 58(3):11:1–11:37, June 2011.
- [3] Chun Du, Jixiang Sun, Shilin Zhou, and Jingjing Zhao. An Outlier Detection Method for Robust Manifold Learning. In Zhixiang Yin, Linqiang Pan, and Xianwen Fang, editors, *Proceedings of The Eighth International Conference on Bio-Inspired Computing: Theories and Applications (BIC-TA), 2013*, Advances in Intelligent Systems and Computing, pages 353–360. Springer Berlin Heidelberg, 2013.
- [4] Sagi Eppel. Using curvature to distinguish between surface reflections and vessel contents in computer vision based recognition of materials in transparent vessels. *arXiv preprint arXiv:1602.00177*, 2006.
- [5] Patrick J Flynn and Anil K Jain. On reliable curvature estimation. *Computer Vision and Pattern Recognition*, 89:110–116, 1989.
- [6] M. Gavish and D. L. Donoho. The optimal hard threshold for singular values is $4/\sqrt{3}$. *IEEE Transactions on Information Theory*, 60(8):5040–5053, Aug 2014.
- [7] David K. Hammond, Pierre Vandergheynst, and Rémi Gribonval. Wavelets on graphs via spectral graph theory. *Applied and Computational Harmonic Analysis*, 30(2):129–150, March 2011.
- [8] Svante Janson. Large deviation inequalities for sums of indicator variables. *arXiv preprint arXiv:1609.00533*, 2016.
- [9] Jianbo Shi and J. Malik. Normalized cuts and image segmentation. *IEEE Transactions on Pattern Analysis and Machine Intelligence*, 22(8):888–905, August 2000.
- [10] Bo. Jiang, Chris. Ding, Bin Luo, and Jin. Tang. Graph-Laplacian PCA: Closed-Form Solution and Robustness. In *2013 IEEE Conference on Computer Vision and Pattern Recognition*, pages 3492–3498, June 2013.
- [11] Shoshichi Kobayashi and Katsumi Nomizu. Foundations of differential geometry. 2, 1996.
- [12] Xiang-Ru Li, Xiao-Ming Li, Hai-Ling Li, and Mao-Yong Cao. Rejecting Outliers Based on Correspondence Manifold. *Acta Automatica Sinica*, 35(1):17–22, January 2009.
- [13] Anna Little, Yuying Xie, and Qiang Sun. An analysis of classical multidimensional scaling. *arXiv preprint arXiv:1812.11954*, 2018.
- [14] G. R. Martin and M. J. Evans. Differentiation of clonal lines of teratocarcinoma cells: formation of embryoid bodies in vitro. *Proceedings of the National Academy of Sciences*, 72(4):1441–1445, April 1975.
- [15] Dereck S. Meek and Desmond J. Walton. On surface normal and gaussian curvature approximations given data sampled from a smooth surface. *Computer Aided Geometric Design*, 17(6):521–543, 2000.

- [16] Marina Meila and Jianbo Shi. Learning Segmentation by Random Walks. In T. K. Leen, T. G. Dietterich, and V. Tresp, editors, *Advances in Neural Information Processing Systems 13*, pages 873–879. MIT Press, 2001.
- [17] Kevin Moon, David van Dijk, Zheng Wang, Scott Gigante, Daniel B. Burkhardt, William S. Chen, Kristina Yim, Antonia van den Elzen, Matthew J. Hirn, Ronald R. Coifman, Natalia B. Ivanova, Guy Wolf, and Smita Krishnaswamy. Visualizing Structure and Transitions for Biological Data Exploration. *bioRxiv*, page 120378, April 2019.
- [18] Helmut Pottmann, Johannes Wallner, Yong-Liang Yang, Yu-Kun Lai, and Shi-Min Hu. Principal curvatures from the integral invariant viewpoint. *Computer Aided Geometric Design*, 24(8):428–442, 2007.
- [19] Ningyu Sha, Ming Yan, and Youzuo Lin. Efficient seismic denoising techniques using robust principal component analysis. In *SEG Technical Program Expanded Abstracts 2019*, pages 2543–2547. Society of Exploration Geophysicists, 2019.
- [20] Wai-Shun Tong and Chi-Keung Tang. Robust estimation of adaptive tensors of curvature by tensor voting. *Pattern Analysis and Machine Intelligence, IEEE Transactions on*, 27(3):434–449, 2005.
- [21] Roman Vershynin. *High-dimensional probability: An introduction with applications in data science*, volume 47. Cambridge University Press, 2018.
- [22] Jinchun Zhan and Namrata Vaswani. Robust pca with partial subspace knowledge. *IEEE Transactions on Signal Processing*, 63(13):3332–3347, 2015.
- [23] Zhigang Tang, Jun Yang, and Bingru Yang. A new Outlier detection algorithm based on Manifold Learning. In *2010 Chinese Control and Decision Conference*, pages 452–457, May 2010.

9 Appendix

This section contains the proof of Theorem 4.2 and the proof of $|\frac{\hat{\lambda}_i - \lambda_i^*}{\lambda_i^*}| \xrightarrow{k \rightarrow \infty} 0$ in §5.

9.1 Proof of Theorem 4.2

Definition 9.1 Let \mathcal{M} be a compact manifold endowed with a continuous measure μ . For any $z \in \mathcal{M}$, its $(\eta(\tau), \tau)$ -neighborhood \mathcal{N} is the neighbourhood with radius $\eta(\tau)$ and measure τ , i.e., $\mu(\mathcal{N}) = \tau$, $\mathcal{N} = \mathcal{M} \cap B_2(z, \eta(\tau))$, and $\eta(\tau) = \min\{r : \mu(\mathcal{M} \cap B_2(z, r)) = \tau\}$.

Since \mathcal{M} is compact, its measure is finite, say $\mu(\mathcal{M}) = A$, and the radii of all the τ -neighbourhoods are bounded by some constant η :

$$\sup_i |\eta_i|^2 \leq \eta^2.$$

Theorem 9.2 (Full version of Theorem 4.2) Given the dataset $X = [X_1, X_2, \dots, X_n]$, let each X_i be independently drawn from a compact manifold $\mathcal{M} \subseteq \mathbb{R}^p$ with intrinsic dimension d and endowed with the uniform distribution μ . Fix some $q > 0$, let $X_{i,j}$, $j = 1, \dots, k_i$ be the k_i points falling in the (η_i, q) -neighbourhood of X_i . Together they form a matrix $X^{(i)} = [X_{i_1}, \dots, X_{i_{k_i}}, X_i]$. Suppose the i.i.d. projections $y_{i,j} \equiv P_{T_{X_i}}(X_{i,j} - X_i)$ where T_{X_i} is the tangent space at X_i obey the same distribution as some a_i for all j , i.e., $y_{i,j} \sim a_i$ (\sim means the two vectors are identically distributed), and the matrix $\mathbb{E}(a_i - \mathbb{E}a_i)(a_i - \mathbb{E}a_i)^*$ has a finite condition number for each i . In addition, suppose the support of the noise matrix $S^{(i)}$ is uniformly distributed among all sets of cardinality m_i . For any $\zeta \in \mathcal{M}$, let T_ζ be the tangent space of \mathcal{M} at ζ and define $\mu_1 := \sup_{\zeta \in \mathcal{M}} \mu(T_\zeta)$. Then as long as $qn \geq c \log n$, $d < \rho_r \min\{nq/2, p\} \mu_1^{-1} \log^{-2} \max\{2nq, p\}$, and $\frac{m_i}{p k_i} \leq 0.4 \rho_s$ (here c , ρ_r and ρ_s are positive numerical constants), then with probability over

$1 - c_1(n \max\{nq/2, p\})^{-10} + \exp(-c_2nq)$ for some constants c_1 and c_2 , the minimizer \hat{S} to (2) with $\lambda_i = \frac{\min\{k_i+1, p\}^{1/2}}{\epsilon_i}$, and $\beta_i = \max\{k_i + 1, p\}^{-1/2}$ has the error bound

$$\sum_i \|\mathcal{P}_i(\hat{S}) - S^{(i)}\|_{2,1} \leq C\sqrt{p\bar{k}}\|\epsilon\|_2.$$

Here $\bar{k} = \max_i k_i$ satisfying $nq/2 \leq \bar{k} \leq 2nq$, $\epsilon_i = \|\tilde{X}^{(i)} - X_i 1^T - T^{(i)} - S^{(i)}\|_F$, $\epsilon = [\epsilon_1, \dots, \epsilon_n]$, $\|\cdot\|_{2,1}$ stands for taking ℓ_2 norm along columns and ℓ_1 norm along the rows, and $T^{(i)}$ is the projection of $X^{(i)} - X_i$ to the tangent space T_{X_i} .

The proof the Theorem 9.2 uses similar techniques as [22]. The main difference is that in [22], both the left and the right singular vectors of the data matrix are required to satisfy the coherence conditions, while here we show that only the left singular vectors that corresponding to the tangent spaces are relevant. In other words, the recovery guarantee is built solely upon assumptions on the intrinsic properties of the manifold, i.e., the tangent spaces.

The proof architecture is as follows. In Section 9.1.1, we derive the error bound in Theorem 4.2 under a small coherence condition for both the left and the right singular vectors of $L^{(i)}$. In Section 9.1.2, we show that the requirement on the right singular vectors can be removed using the i.i.d. assumption on the samples.

9.1.1 Deriving the error bound in Theorem 9.2 under coherence conditions on both the right and the left singular vectors

In Section 3 of the main paper, we explained that $L^{(i)} = X_i 1^T + T^{(i)}$ corresponds to the linear approximation of the i th patch. After the centering $\mathcal{C}(L^{(i)}) = \mathcal{C}(T^{(i)})$, one gets rid of the first term and the resulting matrix has a column span coincide with $T^{(i)}$. This indicates that the columns of $\mathcal{C}(L^{(i)})$ lie in the column space of the tangent space $\text{span}(T^{(i)})$, this also indicates that the rows of $L^{(i)}$ are in $\text{span}\{1^T, T^{(i)}\}$.

One can view the knowledge that 1^T is in the row space of $L^{(i)}$ as a prior knowledge of the left singular vectors of $L^{(i)}$. Robust PCA with prior knowledge is studied in [22], and we will use some of the result therein. Specifically, we adapt the dual certificate approach in [22] to our problem to derive the error bound for our new problem in the theorem, and choose proper λ_i , $i = 1, 2, \dots, n$ and β_i accordingly.

We first state the following assumptions as from [22]:

Assumption A

In each local patch, $L^{(i)} \in \mathbb{R}^{p, k_i+1}$, denote $n_{(1)} = \max\{p, k_i + 1\}$, $n_{(2)} = \min\{p, k_i + 1\}$, let

$$\mathcal{C}(L^{(i)}) = U_i \Sigma_i V_i^*,$$

be the singular value decomposition for each $L^{(i)}$, where $U_i \in \mathbb{R}^{p \times d}$, $\Sigma_i \in \mathbb{R}^{d \times d}$, $V_i^* \in \mathbb{R}^{d \times (k+1)}$. let \tilde{V}_i be the orthonormal basis of $\text{span}\{1, V_i\}$, assume for each $i \in \{1, 2, \dots, n\}$, the following hold with a constant ρ_r that is small enough

$$\max_j \|U_i^* e_j\|^2 \leq \frac{\rho_r d}{p}, \quad (20)$$

$$\max_j \|\tilde{V}_i^* e_j\|^2 \leq \frac{\rho_r d}{k_i}, \quad (21)$$

$$\max_j \|U_i V_i^*\|_\infty \leq \sqrt{\frac{\rho_r d}{pk_i}}. \quad (22)$$

and ρ_r, ρ_s, p, k_i satisfies the following assumptions:

Assumption B([22], Assumption III.2.)

- (a) $\rho_r \leq \min\{10^{-4}, C_1\}$,
- (b) $\rho_s \leq \min\{1 - 1.5b_1(\rho_r), 0.0156\}$,

- (c) $n_{(1)} \geq \max\{C_2(\rho_r), 1024\}$,
- (d) $n_{(2)} \geq 100 \log^2 n_{(1)}$,
- (e) $\frac{(p+k_i)^{1/6}}{\log(p+k_i)} > \frac{10.5}{(\rho_s)^{1/6}(1-5.6561)\sqrt{\rho_s}}$,
- (f) $\frac{pk_i}{500 \log n_{(1)}} > \frac{1}{\rho_s^2}$,

where $b_1(\rho_r), C_2(\rho_r)$ are some constants related to ρ_r .

Denote Π_i as the linear space of matrices for each local patch (note that this is different from the tangent space T^i of the manifold)

$$\Pi_i := \{U_i X^* + Y \tilde{V}_i^*, X \in \mathbb{R}^{p,d}, Y \in \mathbb{R}^{p,d+1}\}.$$

As shown by [22], the following lemma holds, indicating that if incoherence condition is satisfied, then with high probability, there exists desirable dual certificate (W, F) .

Lemma 9.3 ([22], Lemma V.8, Lemma V.9) *For fixed $i = 1, 2, \dots, n$, if assumptions (20), (21), (22), Assumption B and other assumptions in Theorem 9.2 hold, then with probability at least $1 - cn_{(1)}^{-10}$, $\|\mathcal{P}_{\Omega_i} \mathcal{P}_{\Pi_i}\| \leq 1/4$, where Ω_i is the support set of $S^{(i)}$, and $\beta < \frac{3}{10}$. In addition, there exists a pair (W_i, F_i) obeying*

$$U_i V_i^* + W_i = \beta(\text{sgn}(S^{(i)}) + F_i + \mathcal{P}_{\Omega_i} D_i), \quad (23)$$

with

$$\mathcal{P}_{\Pi_i} W_i = 0, \|W_i\| \leq \frac{9}{10}, \mathcal{P}_{\Omega_i} F_i = 0, \|F_i\|_\infty \leq \frac{9}{10}, \|\mathcal{P}_{\Omega_i} D_i\|_F \leq \frac{1}{4}. \quad (24)$$

Therefore, by union bound, with probability over $1 - c n n_{(1)}^{-10}$, for each local patch, there exists a pair (W_i, F_i) obeying (23) and (24).

In Section 9.1.2, we will show that with our assumption that data is independently drawn from a manifold $\mathcal{M} \subseteq \mathbb{R}^p$ with intrinsic dimension d endowed with the uniform distribution, (21) and (22) are satisfied with high probability, so we only need Assumption B and (20), which is only related to the property of tangent space of the manifold itself.

In Lemma 9.5, we prove that in our setting that each X_i is drawn from a manifold $\mathcal{M} \subseteq \mathbb{R}^p$ independently and uniformly, with high probability, for all $i = 1, 2, \dots, n$, k_i is some integer within the range $[qn/2, 2qn]$. Now we use that to prove Theorem 9.2, the result is stated in the following lemma.

Lemma 9.4 *If for all local patch $i = 1, 2, \dots, n$, there exists a pair (W_i, F_i) obeying (23) and (24), then the minimizer \hat{S} to (2) with $\lambda_i = \frac{\min\{k_i+1, p\}^{1/2}}{\epsilon_i}$, and $\beta_i = \max\{k_i + 1, p\}^{-1/2}$ has the error bound*

$$\sum_i \|\mathcal{P}_i(\hat{S}) - S^{(i)}\|_{2,1} \leq C \sqrt{pnk} \|\epsilon\|_2.$$

Here $\epsilon_i = \|\tilde{X}^{(i)} - X_i 1^T - T^{(i)} - S^{(i)}\|_F$, $\epsilon = [\epsilon_1, \dots, \epsilon_n]$ is defined same as Theorem 9.2.

Proof: To simplify notation, let's start with the problem for only one local patch:

$$\min \lambda \|\tilde{X} - L - S\|_F^2 + \|LG\|_* + \beta \|S\|_1. \quad (25)$$

Here $\tilde{X} \in \mathbb{R}^{p \times (k+1)}$, where k denotes the number of neighbors in each local patch, $G = I - \frac{1}{k+1} \mathbf{1}\mathbf{1}^T$ is the centering matrix, recall that the noisy data \tilde{X} is $\tilde{X} = X + S + E = L + R + S + E$, $\|R + E\|_F = \|\tilde{X} - L - S\|_F \leq \epsilon$ (to be more accurate, ϵ_i for patch i), X is the clean data on the manifold, L is first order Talor approximation of X , R is higher order terms, and E denotes random noise. Also denote the solution to problem (25) as $\hat{L} = L + H_1, \hat{S} = S + H_2$. We choose $\beta = \frac{1}{\sqrt{n_{(1)}}} = \frac{1}{\sqrt{\max\{k+1, p\}}}$.

Since \hat{L} , \hat{S} are the solution to (25), the following holds:

$$\begin{aligned}
& \lambda \|\tilde{X} - L - S\|_F^2 + \|LG\|_* + \beta \|S\|_1 \\
& \geq \lambda \|\tilde{X} - (L + H_1) - (S + H_2)\|_F^2 + \|(L + H_1)G\|_* + \beta \|S + H_2\|_1 \\
& \geq \lambda \|H_1 + H_2 - (R + E)\|_F^2 + \|LG\|_* + \langle H_1G, UV^* + W_0 \rangle + \beta \|S\|_1 + \beta \langle H_2, \text{sgn}(S) + F_0 \rangle \\
& = \lambda \|H_1 + H_2\|_F^2 + \lambda \|R + E\|_F^2 - 2\lambda \langle R + E, H_1 + H_2 \rangle + \|LG\|_* + \langle H_1G, UV^* \rangle + \beta \|S\|_1 \\
& \quad + \beta \langle H_2, \text{sgn}(S) \rangle + \|\mathcal{P}_{\Pi^\perp}(H_1G)\|_* + \beta \|\mathcal{P}_{\Omega^\perp}H_2\|_1.
\end{aligned}$$

Here we choose W_0 and F_0 such that $\langle H_1G, W_0 \rangle = \|\mathcal{P}_{\Pi^\perp}(H_1G)\|_*$, $\langle H_2, F_0 \rangle = \|\mathcal{P}_{\Omega^\perp}H_2\|_1$ same as [2]. Note that $LG = U\Sigma V^*$, $G = I - \frac{1}{k+1}\mathbf{1}\mathbf{1}^T$ is orthogonal projector, $LG\mathbf{1} = 0$ implies $V^*\mathbf{1} = 0$, we have

$$\langle H_1G, UV^* \rangle = \langle H_1, UV^*G \rangle = \langle H_1, UV^*(I - \frac{1}{k+1}\mathbf{1}\mathbf{1}^T) \rangle = \langle H_1, UV^* \rangle,$$

$$\mathcal{P}_{\Pi^\perp}(H_1G) = (I - UU^*)H_1G(I - \tilde{V}\tilde{V}^*) = (I - UU^*)H_1(I - \frac{1}{k+1}\mathbf{1}\mathbf{1}^T)(I - \tilde{V}\tilde{V}^*) = \mathcal{P}_{\Pi^\perp}H_1.$$

For the second equality we use the fact that $\mathbf{1}$ lies on the subspace spanned by \tilde{V} , so $(I - \tilde{V}\tilde{V}^*)\mathbf{1} = 0$. And for any matrix M , $\mathcal{P}_{\Pi^\perp}M = (I - UU^*)M(I - \tilde{V}\tilde{V}^*)$.

Denote $H = H_1 + H_2$, plug in the equations above, we obtain

$$\begin{aligned}
2\lambda \langle R + E, H \rangle & \geq \lambda \|H\|_F^2 + \langle H_1 + H_2, UV^* \rangle + \langle H_2, \beta \text{sgn}(S) - UV^* \rangle + \|\mathcal{P}_{\Pi^\perp}H_1\|_* + \beta \|\mathcal{P}_{\Omega^\perp}H_2\|_1 \\
& \geq \lambda \|H\|_F^2 - \|H\|_F \|UV^*\|_F + \langle H_2, W - \beta F - \beta \mathcal{P}_\Omega D \rangle + \|\mathcal{P}_{\Pi^\perp}H_1\|_* + \beta \|\mathcal{P}_{\Omega^\perp}H_2\|_1 \\
& \geq \lambda \|H\|_F^2 - \sqrt{n_{(2)}} \|H\|_F - \frac{9}{10} \|\mathcal{P}_{\Pi^\perp}H_2\|_* - \frac{9}{10} \beta \|\mathcal{P}_{\Omega^\perp}H_2\|_1 - \frac{\beta}{4} \|\mathcal{P}_\Omega H_2\|_F + \\
& \quad \|\mathcal{P}_{\Pi^\perp}H_1\|_* + \beta \|\mathcal{P}_{\Omega^\perp}H_2\|_1.
\end{aligned}$$

In the 3rd inequality we used

$$\begin{aligned}
|\langle H_2, W \rangle| & = |\langle H_2, \mathcal{P}_{\Pi^\perp}W \rangle| = |\langle \mathcal{P}_{\Pi^\perp}H_2, W \rangle| \leq \|\mathcal{P}_{\Pi^\perp}H_2\|_* \|W\| \leq \frac{9}{10} \|\mathcal{P}_{\Pi^\perp}H_2\|_*, \\
|\langle H_2, F \rangle| & = |\langle H_2, \mathcal{P}_{\Omega^\perp}F \rangle| = |\langle \mathcal{P}_{\Omega^\perp}H_2, F \rangle| \leq \|\mathcal{P}_{\Omega^\perp}H_2\|_1 \|F\|_\infty \leq \frac{9}{10} \|\mathcal{P}_{\Omega^\perp}H_2\|_1, \\
|\langle H_2, \mathcal{P}_\Omega D \rangle| & \leq |\langle \mathcal{P}_\Omega H_2, \mathcal{P}_\Omega D \rangle| \leq \frac{1}{4} \|\mathcal{P}_\Omega H_2\|_F.
\end{aligned}$$

Assume $\|R + E\|_F \leq \epsilon$, for all $i = 1, 2, \dots, n$. Also note that

$$\begin{aligned}
\|\mathcal{P}_\Omega H_2\|_F & \leq \|\mathcal{P}_\Omega \mathcal{P}_\Pi H_2\|_F + \|\mathcal{P}_\Omega \mathcal{P}_{\Pi^\perp} H_2\|_F \\
& \leq \frac{1}{4} \|H_2\|_F + \|\mathcal{P}_{\Pi^\perp} H_2\|_F \\
& \leq \frac{1}{4} \|\mathcal{P}_\Omega H_2\|_F + \frac{1}{4} \|\mathcal{P}_{\Omega^\perp} H_2\|_F + \|\mathcal{P}_{\Pi^\perp} H_2\|_F,
\end{aligned}$$

then we have

$$\|\mathcal{P}_\Omega H_2\|_F \leq \frac{1}{3} \|\mathcal{P}_{\Omega^\perp} H_2\|_F + \frac{4}{3} \|\mathcal{P}_{\Pi^\perp} H_2\|_F \leq \frac{1}{3} \|\mathcal{P}_{\Omega^\perp} H_2\|_1 + \frac{4}{3} \|\mathcal{P}_{\Pi^\perp} H_2\|_*.$$

Plug into the previous inequality, also note that for $n_{(1)} \geq 16$, $\beta = \frac{1}{\sqrt{n_{(1)}}} \leq \frac{1}{4}$, it gives

$$\begin{aligned}
2\lambda \epsilon \|H\|_F & \geq \lambda \|H\|_F^2 - \sqrt{n_{(2)}} \|H\|_F - \left(\frac{9}{10} + \frac{\beta}{3}\right) \|\mathcal{P}_{\Pi^\perp}H_2\|_* + \frac{\beta}{60} \|\mathcal{P}_{\Omega^\perp}H_2\|_1 + \|\mathcal{P}_{\Pi^\perp}H_1\|_* \\
& \geq \lambda \|H\|_F^2 - \sqrt{n_{(2)}} \|H\|_F + \frac{\beta}{60} \|\mathcal{P}_{\Omega^\perp}H_2\|_1 + \frac{1}{60} \|\mathcal{P}_{\Pi^\perp}H_1\|_* + \frac{59}{60} (\|\mathcal{P}_{\Pi^\perp}H_1\|_* - \|\mathcal{P}_{\Pi^\perp}H_2\|_*) \\
& = \lambda \|H\|_F^2 - \sqrt{n_{(2)}} \|H\|_F + \frac{\beta}{60} \|\mathcal{P}_{\Omega^\perp}H_2\|_1 + \frac{1}{60} \|\mathcal{P}_{\Pi^\perp}H_1\|_* + \frac{59}{60} (\|\mathcal{P}_{\Pi^\perp}H_1\|_* - \|\mathcal{P}_{\Pi^\perp}(-H_2)\|_*) \\
& \geq \lambda \|H\|_F^2 - \sqrt{n_{(2)}} \|H\|_F + \frac{\beta}{60} \|\mathcal{P}_{\Omega^\perp}H_2\|_1 + \frac{1}{60} \|\mathcal{P}_{\Pi^\perp}H_1\|_* - \frac{59}{60} \|\mathcal{P}_{\Pi^\perp}(H_1 + H_2)\|_* \\
& \geq \lambda \|H\|_F^2 - \sqrt{n_{(2)}} \|H\|_F + \frac{\beta}{60} \|\mathcal{P}_{\Omega^\perp}H_2\|_1 + \frac{1}{60} \|\mathcal{P}_{\Pi^\perp}H_1\|_* - \|H\|_*.
\end{aligned}$$

The last inequality is due to

$$\|\mathcal{P}_{\Pi^\perp} H\|_* = \sup_{\|X\|_2 \leq 1} \langle \mathcal{P}_{\Pi^\perp} H, X \rangle = \sup_{\|X\|_2 \leq 1} \langle H, \mathcal{P}_{\Pi^\perp} X \rangle \leq \sup_{\|\mathcal{P}_{\Pi^\perp} X\|_2 \leq 1} \langle H, \mathcal{P}_{\Pi^\perp} X \rangle \leq \sup_{\|X\|_2 \leq 1} \langle H, X \rangle = \|H\|_*.$$

Note that $\|H\|_* \leq \sqrt{n(2)}\|H\|_F$, then we obtain

$$2\lambda\epsilon\|H\|_F \geq \lambda\|H\|_F^2 - 2\sqrt{n(2)}\|H\|_F + \frac{\beta}{60}\|\mathcal{P}_{\Omega^\perp} H_2\|_1 + \frac{1}{60}\|\mathcal{P}_{\Pi^\perp} H_1\|_*.$$

Rewrite this inequality gives

$$\begin{aligned} \frac{\beta}{60}\|\mathcal{P}_{\Omega^\perp} H_2\|_1 + \frac{1}{60}\|\mathcal{P}_{\Pi^\perp} H_1\|_* &\leq -\lambda\|H\|_F^2 + 2(\sqrt{n(2)} + \lambda\epsilon)\|H\|_F \\ &= -\lambda(\|H\|_F - (\frac{\sqrt{n(2)} + \lambda\epsilon}{\lambda}))^2 + (\frac{\sqrt{n(2)}}{\sqrt{\lambda}} + \sqrt{\lambda}\epsilon)^2 \\ &\leq (\frac{\sqrt{n(2)}}{\sqrt{\lambda}} + \sqrt{\lambda}\epsilon)^2. \end{aligned}$$

Recall that in our original optimization problem, we should consider above inequalities for the summation of all the local patches, denote $h_i \equiv \|H^{(i)}\|_F$, then

$$\begin{aligned} &\sum_{i=1}^n \frac{\beta_i}{60}\|\mathcal{P}_{\Omega_i^\perp} H_2^{(i)}\|_1 + \frac{1}{60}\sum_{i=1}^n \|\mathcal{P}_{\Pi_i^\perp} H_1^{(i)}\|_* \\ &\leq \sum_{i=1}^n -\lambda_i\|H^{(i)}\|_F^2 + 2\sqrt{\min\{k_i + 1, p\}}\|H^{(i)}\|_F + 2\lambda_i\epsilon_i\|H^{(i)}\|_F \\ &= \sum_{i=1}^n -\lambda_i h_i^2 + 2\sqrt{\min\{k_i + 1, p\}}h_i + 2\lambda_i\epsilon_i h_i \\ &= \sum_{i=1}^n -\lambda_i(h_i - \frac{\sqrt{\min\{k_i + 1, p\}} + \lambda_i\epsilon_i}{\lambda_i})^2 + (\frac{\sqrt{\min\{k_i + 1, p\}}}{\sqrt{\lambda_i}} + \sqrt{\lambda_i}\epsilon_i)^2 \\ &\leq 4\sum_{i=1}^n \sqrt{\min\{k_i + 1, p\}}\epsilon_i, \end{aligned}$$

where we choose $\lambda_i = \frac{\sqrt{\min\{k_i + 1, p\}}}{\epsilon_i}$, and $\beta_i = \frac{1}{\sqrt{\max\{k_i + 1, p\}}}$.

Then we have the bound for $\sum_{i=1}^n \|\mathcal{P}_{\Pi_i^\perp} H_1^{(i)}\|_*$ and $\sum_{i=1}^n \|\mathcal{P}_{\Omega_i^\perp} H_2^{(i)}\|_1$

$$\begin{aligned} \sum_{i=1}^n \|\mathcal{P}_{\Pi_i^\perp} H_1^{(i)}\|_* &\leq C\sqrt{\min\{\bar{k}, p\}}\sum_{i=1}^n \epsilon_i \leq C\sqrt{\min\{\bar{k}, p\}}\sqrt{n}\|\epsilon\|_2, \\ \sum_{i=1}^n \|\mathcal{P}_{\Omega_i^\perp} H_2^{(i)}\|_1 &\leq C\sqrt{\max_i \max\{k_i, p\}}\sum_{i=1}^n \sqrt{\min\{k_i, p\}}\epsilon_i \\ &= C\sqrt{\max\{\bar{k}, p\}}\sum_{i=1}^n \sqrt{\min\{k_i, p\}}\epsilon_i \\ &\leq C\sqrt{\max\{\bar{k}, p\}}\min\{\bar{k}, p\}\sum_{i=1}^n \epsilon_i \\ &\leq C\sqrt{p\bar{k}}\sqrt{n}\|\epsilon\|_2. \end{aligned}$$

Denote $H_2^{(i)} \equiv \mathcal{P}_i(\hat{S}) - S^{(i)}$, to estimate the error bound of $\sum_{i=1}^n \|H_2^{(i)}\|_{2,1}$, we decompose $H_2^{(i)}$ into three parts, for each $i = 1, 2, \dots, n$

$$\begin{aligned} \|H_2^{(i)}\|_F &\leq \|(I - \mathcal{P}_{\Omega_i})H_2^{(i)}\|_F + \|(\mathcal{P}_{\Omega_i} - \mathcal{P}_{\Omega_i}\mathcal{P}_{\Pi_i})H_2^{(i)}\|_F + \|\mathcal{P}_{\Omega_i}\mathcal{P}_{\Pi_i}H_2^{(i)}\|_F \\ &\leq \|\mathcal{P}_{\Omega_i^\perp}H_2^{(i)}\|_F + \|\mathcal{P}_{\Pi_i^\perp}H_2^{(i)}\|_F + \frac{1}{4}\|H_2^{(i)}\|_F, \end{aligned}$$

which leads to

$$\begin{aligned} \|H_2^{(i)}\|_F &\leq \frac{4}{3}(\|\mathcal{P}_{\Omega_i^\perp}H_2^{(i)}\|_F + \|\mathcal{P}_{\Pi_i^\perp}H_2^{(i)}\|_F) \\ &= \frac{4}{3}(\|\mathcal{P}_{\Omega_i^\perp}H_2^{(i)}\|_1 + \|\mathcal{P}_{\Pi_i^\perp}H_1^{(i)}\|_* + \|\mathcal{P}_{\Pi_i^\perp}H^{(i)}\|_F) \\ &\leq \frac{4}{3}(\|\mathcal{P}_{\Omega_i^\perp}H_2^{(i)}\|_1 + \|\mathcal{P}_{\Pi_i^\perp}H_1^{(i)}\|_* + \|H^{(i)}\|_F). \end{aligned}$$

Next, we need to bound $\sum_{i=1}^n \|H^{(i)}\|_F$, note that $\lambda_i = \frac{\sqrt{\min\{k_i+1, p\}}}{\epsilon_i}$ and

$$\sum_{i=1}^n -\lambda_i h_i^2 + 2\sqrt{\min\{k_i+1, p\}}h_i + 2\lambda_i \epsilon_i h_i \geq 0,$$

which gives

$$4\sqrt{\min\{\bar{k}+1, p\}} \sum_{i=1}^n h_i \geq 4 \sum_{i=1}^n \sqrt{\min\{k_i+1, p\}}h_i \geq \sum_{i=1}^n \sqrt{\min\{k_i+1, p\}} \frac{h_i^2}{\epsilon_i} \geq \sqrt{\min\{\underline{k}+1, p\}} \sum_{i=1}^n \frac{h_i^2}{\epsilon_i},$$

by Cauchy inequality

$$\sum_{i=1}^n \frac{h_i^2}{\epsilon_i} \geq \frac{(\sum_{i=1}^n h_i)^2}{\sum_{i=1}^n \epsilon_i} \geq \frac{(\sum_{i=1}^n h_i)^2}{\sqrt{n}\|\epsilon\|_2},$$

then we obtain

$$\sum_{i=1}^n h_i \leq 4\sqrt{\frac{\min\{\bar{k}+1, p\}}{\min\{\underline{k}+1, p\}}} \sqrt{n}\|\epsilon\|_2 \leq C\sqrt{n}\|\epsilon\|_2,$$

the last inequality is due to $\frac{nq}{2} \leq \underline{k} \leq \bar{k} \leq 2nq$, which is guaranteed with high probability by Lemma 9.5, thus

$$\begin{aligned} \sum_{i=1}^n \|H_2^{(i)}\|_F &\leq \frac{4}{3} \left(\sum_{i=1}^n \|\mathcal{P}_{\Omega_i^\perp}H_2^{(i)}\|_1 + \sum_{i=1}^n \|\mathcal{P}_{\Pi_i^\perp}H_1^{(i)}\|_* + \sum_{i=1}^n \|H^{(i)}\|_F \right) \\ &= \frac{4}{3} \left(\sum_{i=1}^n \|\mathcal{P}_{\Omega_i^\perp}H_2^{(i)}\|_1 + \sum_{i=1}^n \|\mathcal{P}_{\Pi_i^\perp}H_1^{(i)}\|_* + \sum_{i=1}^n h_i \right) \\ &\leq C\sqrt{p\bar{k}n}\|\epsilon\|_2. \end{aligned}$$

Now let's divide $H_2^{(i)}$ into columns to get the $\ell_{2,1}$ norm error bound, denote $(H_2^{(i)})_j$ as the j th column in $H_2^{(i)}$, then we can derive the $\ell_{2,1}$ norm error bound in Lemma 9.4

$$\begin{aligned} C\sqrt{p\bar{k}n}\|\epsilon\|_2 &\geq \sum_{i=1}^n \|H_2^{(i)}\|_F = \sum_{i=1}^n \sqrt{\sum_{j=1}^{k_i+1} \|(H_2^{(i)})_j\|_2^2} \\ &\gtrsim \sum_{i=1}^n \sqrt{\frac{1}{k_i} \left(\sum_{j=1}^{k_i} \|(H_2^{(i)})_j\|_2 \right)^2} \\ &\gtrsim \frac{1}{\sqrt{\bar{k}}} \sum_{i=1}^n \sum_{j=1}^{k_i} \|(H_2^{(i)})_j\|_2. \end{aligned}$$

Then we obtain

$$\sum_i \|\mathcal{P}_i(\hat{S}) - S^{(i)}\|_{2,1} = \sum_{i=1}^n \sum_{j=1}^{k_i+1} \|(H_2^{(i)})_j\|_2 \leq C\sqrt{pmk}\|\epsilon\|_2.$$

□

Lemma 9.5 *If $qn \geq 9 \log n$, with probability at least $1 - 2 \exp(-c_3 qn)$, $\frac{qn}{2} \leq k_i \leq 2qn$, for all $i = 1, 2, \dots, n$, here c_3 is some constants not related to q and n .*

Proof: Since each X_i is drawn from a manifold $\mathcal{M} \subseteq \mathbb{R}^p$ independently and uniformly, for some fixed (η_{i_0}, q) -neighborhood of X_{i_0} , for each $j = \{1, 2, \dots, n\} \setminus \{i_0\}$, the probability that X_j falls into (η_{i_0}, q) -neighborhood is q . Since $\{X_i\}_{i=1,2,\dots,n}$, k_i follows i.i.d binomial distribution $B(n, q)$, we can apply large deviations inequalities to derive an upper and lower bound for k_i . By Theorem 1 in [8], we have that for each $i = 1, 2, \dots, n$

$$\begin{aligned} \mathbb{P}(k_i > 2qn) &\leq \exp\left(-\frac{(qn)^2}{2(qn(1-q) + qn/3)}\right) \leq \exp\left(-\frac{3}{8}qn\right), \\ \mathbb{P}(k_i < \frac{qn}{2}) &\leq \exp\left(-\frac{(qn/2)^2}{2qn}\right) = \exp\left(-\frac{1}{8}qn\right). \end{aligned}$$

Therefore by Union Bound Theorem

$$\begin{aligned} \mathbb{P}\left(\frac{qn}{2} \leq k_i \leq 2qn, \forall i = 1, 2, \dots, n\right) &\geq 1 - n(\exp(-\frac{3}{8}qn) + \exp(-\frac{1}{8}qn)) \\ &\geq 1 - 2n \exp(-\frac{1}{8}qn) \\ &= 1 - 2 \exp(-\frac{1}{8}qn + \log n) \\ &\geq 1 - 2 \exp(-\frac{1}{72}qn). \end{aligned}$$

□

9.1.2 Removing (21) and (22) in Assumption A

We will show that under our assumption that points are uniformly drawn from the manifold, (21) and (22) in Assumption A automatically hold provided (20) holds, thus they can be removed from the requirements.

Let us again restrict our attention to an individual patch and for the simplicity of notation, ignore the superscript i (the treatment for all patches are the same). Recall that $\mathcal{C}(L) = \mathcal{C}(T) = U\Sigma V^*$, and \tilde{V} is the orthonormal basis of $\text{span}([1, V])$, since $0 = \mathcal{C}(T)\mathbf{1} = U\Sigma V^*\mathbf{1}$, we have $V^*\mathbf{1} = 0$, then $\mathbf{1} \perp \text{span}(V)$, thus we can write one basis for $\text{span}([1, V])$ as $[\frac{1}{\sqrt{k+1}}\mathbf{1}, V]$, which indicates that in order to remove (21), we only need to show that with high probability, V has small coherence. Also, recall that $T^{(i)} = P_{T_{X_i}}(X^{(i)} - X_i\mathbf{1}^T)$, since each X_i is independent, each column in $T^{(i)}$ is also independent. In addition, each column is in the span of the tangent space with U being an orthonormal basis. Therefore $T = U\Lambda \equiv U[\alpha_1, \alpha_2, \dots, \alpha_k, 0]$, where $\alpha_i, i = 1, 2, \dots, k$ is the i th column of Λ , which corresponds to the coefficients of the i th column of T under U , the last column is zero vector since it corresponds to X_i itself. Since columns of T are i.i.d, then α_i s are also i.i.d., so they all obey the same distribution as a random vector α . We establish the following lemma for the right singular vectors of T .

Lemma 9.6 *Let $\mathcal{C}(T) = U\Sigma V^*$ be the reduced singular vector decomposition of $\mathcal{C}(T)$, assume $C \equiv \mathbb{E}((\alpha - \mathbb{E}\alpha)(\alpha - \mathbb{E}\alpha)^*)$ has a finite condition number. Then, with probability at least $1 - 2d \exp(-ck)$, the right singular vector V obeys*

$$\max_{1 \leq j \leq k} \|V^* \mathbf{e}_j\|^2 \leq \frac{c}{k},$$

and with (1) in Assumption A

$$\|UV^*\|_\infty \leq \sqrt{\frac{cd}{pk}}.$$

Proof: As discussed above, $\mathcal{C}(T)$ has the following representation

$$\mathcal{C}(T) = TG = U[\alpha_1, \alpha_2, \dots, \alpha_k, \mathbf{0}]G,$$

where $U \in \mathbb{R}^{p,d}$ is an orthonormal basis of the tangent space, and $\Lambda = [\alpha_1, \alpha_2, \dots, \alpha_k, \mathbf{0}] \in \mathbb{R}^{d,k+1}$ is the coefficients of randomly drawn points in a neighbourhood projected to the tangent space.

Since points are randomly drawn from an neighbourhood contained in a ball of radius at most η , one can easily verify that $\|\alpha_j\|_2 \leq \eta$ for each $j = 1, \dots, k$. Assume TG and Λ have the reduced SVD of the form

$$TG = U\Sigma V^*, \quad \Lambda G = U_\Lambda \Sigma_\Lambda V_\Lambda^*,$$

Then T can be written as

$$TG = U\Sigma V^* = UU_\Lambda \Sigma_\Lambda V_\Lambda^*.$$

It can be verified that $\text{null}(TG)$ is the span of columns in $(V_\Lambda)^C$, then we have $\text{span}(V_\Lambda) = \text{span}(V)$, since both V_Λ and V are orthonormal, they are equal up to a rotation, i.e. $\exists R \in \mathbb{R}^{d,d}$, $R^*R = RR^* = I$, such that $V = V_\Lambda R$. Then

$$\max_{1 \leq j \leq k} \|V^* \mathbf{e}_j\|^2 = \max_{1 \leq j \leq k} \|R^* V_\Lambda^* \mathbf{e}_j\|^2 = \max_{1 \leq j \leq k} \|V_\Lambda^* \mathbf{e}_j\|^2.$$

Next we bound the coherence of V_Λ . Since $V_\Lambda^* = \Sigma_\Lambda^{-1} U_\Lambda^* \Lambda G$, we have

$$\begin{aligned} \max_{1 \leq j \leq k} \|\Sigma_\Lambda^{-1} U_\Lambda^* \Lambda G \mathbf{e}_j\| &\leq \|\Sigma_\Lambda^{-1}\| \max_{1 \leq i \leq k} \|U_\Lambda^* \Lambda G \mathbf{e}_j\| \\ &= \|\Sigma_\Lambda^{-1}\| \max_{1 \leq j \leq k} \|\Lambda G \mathbf{e}_j\| \\ &\leq \|\Sigma_\Lambda^{-1}\| \max_{1 \leq j \leq k} \|\alpha_j - \bar{\alpha}\| \\ &\leq 2\eta \|\Sigma_\Lambda^{-1}\|. \end{aligned}$$

Recall that

$$\begin{aligned} \Lambda G &= [\alpha_1, \alpha_2, \dots, \alpha_k, 0] \left(I - \frac{1}{k+1} \mathbf{1}\mathbf{1}^T \right) \\ &= [\alpha_1 - \bar{\alpha}, \alpha_2 - \bar{\alpha}, \dots, \alpha_k - \bar{\alpha}, -\bar{\alpha}] \\ &= [\alpha_1 - \mathbb{E}\alpha, \alpha_2 - \mathbb{E}\alpha, \dots, \alpha_k - \mathbb{E}\alpha, 0] - [\bar{\alpha} - \mathbb{E}\alpha, \bar{\alpha} - \mathbb{E}\alpha, \dots, \bar{\alpha} - \mathbb{E}\alpha, \bar{\alpha}], \end{aligned}$$

where $\bar{\alpha} = \frac{1}{k+1} \sum_{i=1}^k \alpha_i$, thus

$$\begin{aligned} &|\sigma_d(\Lambda G) - \sigma_d([\alpha_1 - \mathbb{E}\alpha, \alpha_2 - \mathbb{E}\alpha, \dots, \alpha_k - \mathbb{E}\alpha, 0])| \\ &\leq \|[\bar{\alpha} - \mathbb{E}\alpha, \bar{\alpha} - \mathbb{E}\alpha, \dots, \bar{\alpha} - \mathbb{E}\alpha, \bar{\alpha}]\|_2 \\ &\leq \|[\bar{\alpha} - \mathbb{E}\alpha, \bar{\alpha} - \mathbb{E}\alpha, \dots, \bar{\alpha} - \mathbb{E}\alpha, \bar{\alpha} - \mathbb{E}\alpha]\|_2 + \|\mathbb{E}\alpha\|_2 \\ &\leq \sqrt{k+1} \left\| \frac{1}{k+1} \sum_{i=1}^k (\alpha_i - \mathbb{E}\alpha) - \frac{1}{k+1} \mathbb{E}\alpha \right\|_2 + \eta \\ &\leq \frac{1}{\sqrt{k+1}} \sum_{i=1}^k \|\alpha_i - \mathbb{E}\alpha\|_2 + 2\eta \end{aligned} \tag{26}$$

First, we want to use Bernstein Matrix Inequality to bound the ℓ_2 -norm in the last inequality. Denote $\beta_i = \frac{1}{\sqrt{k+1}} (\alpha_i - \mathbb{E}\alpha)$, $Z = \sum_{i=1}^k \beta_i$, then β_i is independent, we also have

$$\mathbb{E}\beta_i = 0, \quad \|\beta_i\|_2 \leq \frac{1}{\sqrt{k+1}} (\|\alpha_i\|_2 + \|\mathbb{E}\alpha\|_2) \leq \frac{2\eta}{\sqrt{k}},$$

which means β_i has mean zero and is uniformly bounded, also

$$\begin{aligned} \nu(Z) &= \max\{\|\mathbb{E}(ZZ^*)\|_2, \|\mathbb{E}(Z^*Z)\|_2\} \\ &= \max\left\{\left\| \sum_{i=1}^k \mathbb{E}(\beta_i \beta_i^*) \right\|_2, \left\| \sum_{i=1}^k \mathbb{E}(\beta_i^* \beta_i) \right\|_2\right\} \\ &= \frac{k}{k+1} \max\{\|\mathbb{E}(\alpha_i - \mathbb{E}\alpha)(\alpha_i - \mathbb{E}\alpha)^T\|_2, \mathbb{E} \text{tr}((\alpha_i - \mathbb{E}\alpha)(\alpha_i - \mathbb{E}\alpha)^T)\} \\ &< \max\{\|C\|_2, \text{tr}(C)\} \\ &< d\sigma_1(C). \end{aligned}$$

By assumption, C has finite condition number, and $d \ll k$, by Matrix Bernstein inequality, we are able to bound the spectral norm of Z

$$P(\|Z\|_2 \geq t) \leq (d+1) \exp\left(\frac{-t^2}{d\sigma_1(C) + \frac{2\eta t}{3\sqrt{k}}}\right)$$

Let $t = \frac{\sqrt{\sigma_d(C)k}}{4}$, we have

$$P(\|Z\|_2 \geq \frac{\sqrt{\sigma_d(C)k}}{4}) \leq d \exp(-ck). \quad (27)$$

Next, equipped with Matrix Bernstein inequality again, we can prove that $\sigma_d([\alpha_1 - \mathbb{E}\alpha, \alpha_2 - \mathbb{E}\alpha, \dots, \alpha_k - \mathbb{E}\alpha, 0])$ concentrates around $\sigma_d(C)$. Note that $\sigma_d^2([\alpha_1 - \mathbb{E}\alpha, \alpha_2 - \mathbb{E}\alpha, \dots, \alpha_k - \mathbb{E}\alpha, 0]) = \sigma_d(\sum_{i=1}^k (\alpha_i - \mathbb{E}\alpha)(\alpha_i - \mathbb{E}\alpha)^T)$, we consider

$$|\sigma_d(\sum_{i=1}^k (\alpha_i - \mathbb{E}\alpha)(\alpha_i - \mathbb{E}\alpha)^T) - k\sigma_d(C)| \leq \|\sum_{i=1}^k (\alpha_i - \mathbb{E}\alpha)(\alpha_i - \mathbb{E}\alpha)^T - kC\|_2$$

Similar as what we discussed above, let $Z_j = (\alpha_j - \mathbb{E}\alpha)(\alpha_j - \mathbb{E}\alpha)^T - C$, $j = 1, 2, \dots, k$. It can be verified that Z_j is bounded

$$\|Z_j\|_2 \leq \|\alpha_j - \mathbb{E}\alpha\|_2^2 + \sigma_1(C) \leq 2\eta^2 + \sigma_1(C) \equiv c_4.$$

Since Z_j follows i.i.d distribution, we also have $\nu(Z) \leq kc_5$ for some constant c_5 which represents the variance of Z_j . Applying matrix Bernstein inequality, we obtain

$$\mathbb{P}\left(\|\sum_{j=1}^k (\alpha_j - \mathbb{E}\alpha)(\alpha_j - \mathbb{E}\alpha)^T - kC\|_2 \geq t\right) \leq 2d \exp\left(-\frac{t^2}{kc_5 + \frac{c_4 t}{3}}\right)$$

further, take $t = \frac{3k\sigma_d(C)}{4}$, then with probability over $1 - 2d \exp(-c_6 k)$ for some constant c_6 , the following holds

$$|\sigma_d(\sum_{i=1}^k (\alpha_i - \mathbb{E}\alpha)(\alpha_i - \mathbb{E}\alpha)^T) - k\sigma_d(C)| \leq \|\sum_{i=1}^k (\alpha_i - \mathbb{E}\alpha)(\alpha_i - \mathbb{E}\alpha)^T - kC\|_2 < \frac{3k\sigma_d(C)}{4},$$

which leads to

$$\sigma_d^2([\alpha_1 - \mathbb{E}\alpha, \alpha_2 - \mathbb{E}\alpha, \dots, \alpha_k - \mathbb{E}\alpha]) = \sigma_d(\sum_{i=1}^k (\alpha_i - \mathbb{E}\alpha)(\alpha_i - \mathbb{E}\alpha)^T) > \frac{k\sigma_d(C)}{4},$$

thus

$$\sigma_d([\alpha_1 - \mathbb{E}\alpha, \alpha_2 - \mathbb{E}\alpha, \dots, \alpha_k - \mathbb{E}\alpha]) > \frac{\sqrt{k\sigma_d(C)}}{2}. \quad (28)$$

Combine (26), (27) and (28), we have proved that with probability at least $1 - d \exp(-ck)$, $\sigma_d(\Lambda P) \gtrsim \sqrt{k}$, therefore $\|\Sigma_\Lambda^{-1}\| \lesssim \frac{1}{\sqrt{k}}$, which further gives $\max_{1 \leq j \leq k+1} \|V^* \mathbf{e}_j\|^2 \lesssim \frac{1}{k}$.

Finally, with (20) in Assumption A, (22) is also satisfied with the same probability, since

$$\|UV^*\|_\infty \leq \max_j \|U^* \mathbf{e}_j\|_2 \max_l \|V^* \mathbf{e}_l\|_2 \leq \sqrt{\frac{cd}{pk}}.$$

Hence (22) in Assumption A can also be removed. \square

The above discussion is valid for each patch individually, i.e., with probability at least $1 - d \exp(-ck_i) \geq 1 - d \exp(-ck)$, (21) and (22) hold for any fixed $i = 1, 2, \dots, n$. By union bound inequality, with probability at least $1 - nd \exp(-ck)$, (21) and (22) hold for all the local patches.

Note that $1 - nd \exp(-ck) = 1 - \exp(-ck + \log n)$, here we omit d since it is very small. By Lemma 9.5, with probability at least $1 - 2 \exp(-c_1 qn)$, $\frac{nq}{2} \leq k_i \leq 2nq$, for all $i = 1, 2, \dots, n$. Using the assumption in Theorem 4.2, $qn \geq c_2 \log n$ for some constant c_2 larger enough, we can see that with probability over $1 - \exp(-c_3 k)$, the requirement (21) and (22) automatically hold due to i.i.d assumption on the samples, which enable us to remove these assumptions in Theorem 4.2.

9.2 Proof of the convergence of $\frac{\hat{\lambda}_i - \lambda_i^*}{\lambda_i^*}$ as $k \rightarrow \infty$

When k is large enough, $\min\{k+1, p\} = p$, $\hat{\lambda}_i = \frac{\sqrt{p}}{\hat{\epsilon}_i}$, $\lambda_i^* = \frac{\sqrt{p}}{\epsilon_i}$, then

$$\frac{\hat{\lambda}_i - \lambda_i^*}{\lambda_i^*} = \frac{\frac{\sqrt{p}}{\hat{\epsilon}_i} - \frac{\sqrt{p}}{\epsilon_i}}{\frac{\sqrt{p}}{\epsilon_i}} = \frac{\epsilon_i - \hat{\epsilon}_i}{\hat{\epsilon}_i} = \frac{\epsilon_i}{\hat{\epsilon}_i} - 1.$$

In order to show $|\frac{\hat{\lambda}_i - \lambda_i^*}{\lambda_i^*}| \xrightarrow{k \rightarrow \infty} 0$, it is sufficient to prove that $\frac{\epsilon_i^2 - \hat{\epsilon}_i^2}{\hat{\epsilon}_i^2} = \frac{\epsilon_i^2}{\hat{\epsilon}_i^2} - 1 \xrightarrow{k \rightarrow \infty} 0$, thus $\frac{\epsilon_i}{\hat{\epsilon}_i} \xrightarrow{k \rightarrow \infty} 1$, hence $\frac{\hat{\lambda}_i - \lambda_i^*}{\lambda_i^*} \xrightarrow{k \rightarrow \infty} 0$. Notice that

$$\begin{aligned} \left| \frac{\epsilon_i^2 - \hat{\epsilon}_i^2}{\hat{\epsilon}_i^2} \right| &= \left| \frac{\|R^{(i)} + N^{(i)}\|_F^2 - ((k+1)p\sigma^2 + \sum_{j=1}^k \frac{\|X_i - X_{i_j}\|_2^4}{4} \bar{\Gamma}^2(X_i))}{(k+1)p\sigma^2 + \sum_{j=1}^k \frac{\|X_i - X_{i_j}\|_2^4}{4} \bar{\Gamma}^2(X_i)} \right| \\ &\leq \left| \frac{(\|N^{(i)}\|_F^2 - (k+1)p\sigma^2) + (\|R^{(i)}\|_F^2 - \sum_{j=1}^k \frac{\|X_i - X_{i_j}\|_2^4}{4} \bar{\Gamma}^2(X_i)) + \langle N^{(i)}, R^{(i)} \rangle}{kp\sigma^2} \right| \\ &\leq \left| \frac{\|N^{(i)}\|_F^2 - (k+1)p\sigma^2}{kp\sigma^2} \right| + \left| \frac{\|R^{(i)}\|_F^2 - \sum_{j=1}^k \frac{\|X_i - X_{i_j}\|_2^4}{4} \bar{\Gamma}^2(X_i)}{kp\sigma^2} \right| + \left| \frac{\sum_{j=1}^k \langle N_j^{(i)}, R_j^{(i)} \rangle}{(k+1)p\sigma^2} \right|. \end{aligned}$$

Since each entry in $N^{(i)}$ follows i.i.d. obeying $\mathcal{N}(0, \sigma^2)$, $\langle N_j^{(i)}, R_j^{(i)} \rangle$ are also i.i.d. with $\mathbb{E}(\langle N_j^{(i)}, R_j^{(i)} \rangle) = 0$, by law of large numbers, the first and third term approximates 0 when $k \rightarrow \infty$. Also, by (12) and (13) in §5, the second term also approximates 0, thus $\frac{\epsilon_i^2 - \hat{\epsilon}_i^2}{\hat{\epsilon}_i^2} \xrightarrow{k \rightarrow \infty} 0$.